# The ubiquitin ligase CRL2$^{ZYG11}$ targets cyclin B1 for degradation in a conserved pathway that facilitates mitotic slippage

Riju S. Balachandran,[1]* Cassandra S. Heighington,[2]* Natalia G. Starostina,[1] James W. Anderson,[1] David L. Owen,[1] Srividya Vasudevan,[1] and Edward T. Kipreos[1]

[1]Department of Cellular Biology and [2]Department of Genetics, University of Georgia, Athens, GA 30602

The anaphase-promoting complex/cyclosome (APC/C) ubiquitin ligase is known to target the degradation of cyclin B1, which is crucial for mitotic progression in animal cells. In this study, we show that the ubiquitin ligase CRL2$^{ZYG-11}$ redundantly targets the degradation of cyclin B1 in *Caenorhabditis elegans* and human cells. In *C. elegans*, both CRL2$^{ZYG-11}$ and APC/C are required for proper progression through meiotic divisions. In human cells, inactivation of CRL2$^{ZYG11A/B}$ has minimal effects on mitotic progression when APC/C is active. However, when APC/C is inactivated or cyclin B1 is overexpressed, CRL2$^{ZYG11A/B}$-mediated degradation of cyclin B1 is required for normal progression through metaphase. Mitotic cells arrested by the spindle assembly checkpoint, which inactivates APC/C, often exit mitosis in a process termed "mitotic slippage," which generates tetraploid cells and limits the effectiveness of antimitotic chemotherapy drugs. We show that ZYG11A/B subunit knockdown, or broad cullin–RING ubiquitin ligase inactivation with the small molecule MLN4924, inhibits mitotic slippage in human cells, suggesting the potential for antimitotic combination therapy.

## Introduction

The primary role of the cell cycle is to generate two daughter cells during mitosis that possess equivalent genomic DNA. Mitosis in animal cells requires dramatic reorganization of cellular structure, including the restructuring of the cytoskeleton, the dissolution of the nuclear envelope, and the breakdown of the endoplasmic reticulum and Golgi (Lancaster and Baum, 2014; Jongsma et al., 2015). These cellular reorganizations are initiated by the kinase heterocomplex of the mitotic cyclin, cyclin B1, and Cdk1 (Wieser and Pines, 2015). Cyclin B1–Cdk1 phosphorylates a large number of substrates to initiate mitotic entry and drive mitotic processes (Errico et al., 2010; Kettenbach et al., 2011; Pagliuca et al., 2011). Because the activity of cyclin B1–Cdk1 maintains the mitotic program, the complex must be inactivated to allow cells to exit mitosis (Murray, 1989; Murray et al., 1989).

The cyclin B1–Cdk1 complex is inactivated during metaphase by the degradation of cyclin B1. The multisubunit ubiquitin ligase (E3) anaphase-promoting complex/cyclosome (APC/C) with the activating subunit Cdc20, APC/C$^{Cdc20}$, initiates cyclin B1 degradation after chromosome congression to the metaphase plate (Pines, 2006). Before metaphase, APC/C$^{Cdc20}$ is inactivated by the spindle assembly checkpoint (SAC), which prevents the missegregation of chromosomes by ensuring proper chromosome–spindle connections in metaphase (Musacchio, 2015). The SAC inhibits APC/C$^{Cdc20}$ through the creation of the metaphase checkpoint complex (MCC) that binds and inhibits APC/C$^{Cdc20}$. The MCC is created at kinetochores that are not bound by microtubules or that lack microtubule-induced tension. Once all kinetochores are bound to microtubules with tension, the MCC is no longer created, and the Cdc20 component of MCC that is bound to APC/C$^{Cdc20}$ is degraded by autoubiquitylation, initiating the dissociation of the inhibitory complex (Reddy et al., 2007).

At the metaphase-to-anaphase transition, APC$^{Cdc20}$ targets the ubiquitin-mediated degradation of Securin (Ciosk et al., 1998; Zou et al., 1999). Securin is an inhibitor of the cysteine protease Separase, which cleaves the SCC1 subunit of the cohesin complex that holds sister chromatids together (Uhlmann et al., 1999; Hauf et al., 2001). The degradation of Securin releases Separase that then cleaves cohesin to allow the separation of sister chromatids in response to pulling forces generated by the mitotic spindle.

*R.S. Balachandran and C.S. Heighington contributed equally to this paper.

Correspondence to Edward T. Kipreos: ekipreos@uga.edu

Abbreviations used: APC/C, anaphase-promoting complex/cyclosome; CBOX, cyclin box; CRL, cullin–RING ubiquitin ligase; DIC, differential interference contrast; IP, immunoprecipitation; LLnL, Leu-Leu-norleucinal; MCC, metaphase checkpoint complex; SAC, spindle assembly checkpoint; SNP, single nucleotide polymorphism; *ts*, temperature-sensitive; VSV-G, glycoprotein of vesicular stomatitis virus.



Supplemental material can be found at:
http://doi.org/10.1083/jcb.201601083

The Rockefeller University Press $30.00
J. Cell Biol. Vol. 215 No. 2 151–166
https://doi.org/10.1083/jcb.201601083

Studies in budding yeast indicated that the degradation of mitotic cyclins did not affect the metaphase-to-anaphase transition, but was only important for mitotic exit (Surana et al., 1993). In *Xenopus laevis* cycling extracts, the addition of a nondegradable form of cyclin B1 was initially found not to affect the timing of the metaphase-to-anaphase transition, but instead caused an arrest in telophase (Holloway et al., 1993). However, a later study showed that adding increased levels of nondegradable cyclin B1 to *Xenopus* extract induced a metaphase arrest that was caused by the continued inhibition of Separase despite the degradation of Securin (Stemmann et al., 2001). The inactivation of Separase was associated with its phosphorylation by the nondegradable cyclin B1–Cdk1. In mammalian cells, the expression of a nondegradable cyclin B1, at levels only 20–30% of the endogenous cyclin B1, led to metaphase arrest, providing further evidence that cyclin B1 must be degraded to allow the metaphase-to-anaphase transition (Chang et al., 2003).

Surprisingly, Securin is not essential for viability or fertility in mice (Mei et al., 2001). The phosphorylation of Separase by cyclin B1–Cdk1 is more critical, as mutating the Cdk1 phosphorylation site in just one Separase allele in mice results in infertility and early embryonic lethality caused by premature sister chromatid separation (Huang et al., 2008, 2009). The inhibition of Separase by cyclin B1–Cdk1 was initially attributed to "inhibitory" phosphorylation of Separase. However, the phosphorylation of Separase by cyclin B1–Cdk1 was found to be insufficient for the inactivation of Separase in mammalian cells (Gorr et al., 2005). Rather, cyclin B1–Cdk1 binds and directly inhibits phosphorylated Separase, and this is sufficient to fully inhibit Separase even in the absence of Securin (Gorr et al., 2005; Huang et al., 2005). The degradation of mammalian cyclin B1 is therefore essential for Separase activation, which allows the separation of sister chromatids in anaphase.

Mitotic slippage occurs when cells, which are arrested in mitosis in response to continuous activation of the SAC, exit mitosis as undivided tetraploid cells. Mitotic slippage is a major factor in limiting the effectiveness of widely used antimicrotubule chemotherapy drugs that arrest cells in mitosis by blocking the formation or function of the mitotic spindle (Field et al., 2014). Mitotic slippage not only circumvents the mitotic arrest induced by these drugs, but can also contribute to the genesis of new cancer cells by inducing tetraploidy (Ganem et al., 2007). Mechanistically, mitotic slippage has been linked to the continued degradation of cyclin B1 in the presence of an active checkpoint (Brito and Rieder, 2006).

In this study, we show that the ubiquitin ligase CRL2$^{ZYG\text{-}11}$ degrades cyclin B1 in a conserved pathway that functions parallel to APC/C in both *Caenorhabditis elegans* and human cells. Cullin–RING ubiquitin ligases (CRLs) are multisubunit E3s that include a cullin scaffold and variable substrate receptors (Lydeard et al., 2013). The CRL2$^{ZYG\text{-}11}$ complex is comprised of the cullin CUL2, the RING finger protein Rbx1/Roc1, the adaptor subunit Elongin C, and the substrate receptor ZYG-11 in *C. elegans* or its orthologues ZYG11A and ZYG11B in humans. In human cells, the CRL2$^{ZYG11A/B}$-mediated degradation of cyclin B1 facilitates mitotic slippage in cells in which APC/C is inactive.

## Results

### *C. elegans* CRL2$^{ZYG\text{-}11}$ targets cyclin B1 for ubiquitin-mediated degradation

*C. elegans* ZYG-11 is required for multiple functions in the early embryo, including the separation of sister chromatids during the second meiotic division, the establishment of anterior–posterior polarity, and mitotic chromosome condensation (Liu et al., 2004; Sonneville and Gönczy, 2004; Vasudevan et al., 2007). In an effort to understand how ZYG-11 contributes to these processes, we performed a screen for suppressors of a temperature-sensitive (ts) *zyg-11(ax491ts)* allele (see Materials and methods). One of the suppressor strains that we isolated, *zyg-11(ts)*; *ek14*, displayed significant suppression, with 57.2% of *zyg-11(ts)*; *ek14* embryos hatching at 25°C ($n$ = 600) versus 0.8% for *zyg-11(ts)* embryos ($n$ = 745). Single nucleotide polymorphism (SNP) mapping indicated that the *ek14* strain was a compound suppressor, with alleles contributing to the suppression on chromosomes III, IV, V, and X.

We mapped the suppressor on chromosome IV to a region between genetic map positions +1 to +5.9. Whole-genome sequencing indicated that this region contained a homozygous mutation in the mitotic cyclin *cyb-2.1* that changed the CYB-2.1 amino acid residue 120 from a glutamic acid (E) to a lysine (K). E120 is conserved as either a negatively charged glutamic acid or aspartic acid (D) in all mitotic B cyclins and S phase A cyclins in *C. elegans* and humans, suggesting a structural or functional requirement for a negative charge at position 120 (unpublished data). RNAi inactivates both *cyb-2.1* and its close paralogue *cyb-2.2* rescued *zyg-11(ts)* lethality at the semipermissive temperature of 20°C, indicating that loss of CYB-2.1/2.2 activity suppresses *zyg-11* loss of function (Fig. 1 A).

*zyg-11(ts)* mutants are defective for polar body extrusion during meiosis II (Table S1). RNAi depletion of *cyb-2.1/2.2* partially rescues the extrusion of the second polar body in *zyg-11(ts)* mutants at the nonpermissive temperature of 25°C (Table S1). However, *cyb-2.1/2.2* RNAi failed to rescue two other observable *zyg-11* mutant phenotypes (Vasudevan et al., 2007): severe cortical membrane ruffling at the two-cell stage and granule-free cytoplasmic zones in the zygote (Table S1). The rescue of only a subset of *zyg-11* mutant phenotypes is consistent with the expectation that CRL2$^{ZYG\text{-}11}$ regulates multiple substrates and pathways.

There are four cyclin B genes in *C. elegans*: *cyb-1*, the orthologue of human cyclin B1; *cyb-3*, the orthologue of human cyclin B3; and two cyclin B2 paralogues, *cyb-2.1* and *cyb-2.2*, that are closely related to each other (91% aa identity) and are most closely related to cyclin B1 in humans. We observed that both *cyb-1* RNAi and *cyb-2.1/2.2* RNAi were able to suppress *zyg-11(ts)* lethality to similar levels (Fig. 1 A). This suggests that an overall decrease in mitotic cyclin B activity can suppress the *zyg-11* mutant phenotype. *cyb-3* RNAi increased *zyg-11(ts)* embryonic lethality, which can be attributed to the loss of *cyb-3*'s essential role in meiosis II (van der Voet et al., 2009; Deyter et al., 2010).

CUL-2 and ZYG-11 are required for CYB-1 and CYB-3 degradation during the meiotic divisions immediately after fertilization (Liu et al., 2004; Sonneville and Gönczy, 2004). It was unclear whether CRL2$^{ZYG\text{-}11}$ directly targeted the degradation of

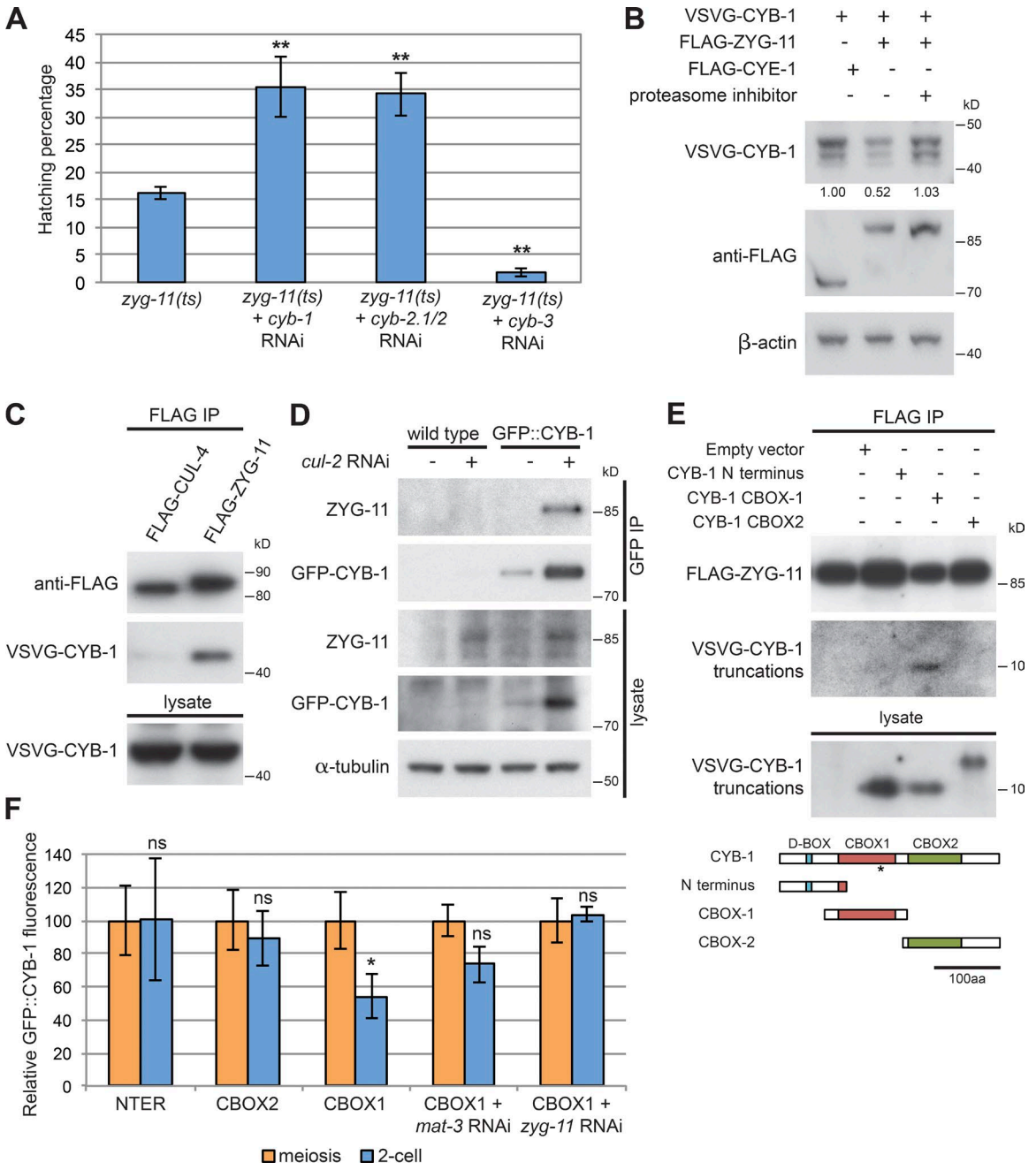


Figure 1. ***C. elegans*CYB-1 is a direct substrate of the CRL2$^{ZYG-11}$ complex.** (A) Egg hatching percentage ± SEM for *zyg-11(ts)* at the semipermissive temperature of 20°C with the listed RNAi treatments; from at least three independent counts, with the total number of embryos analyzed (from left to right): 667, 1,163, 448, and 222, respectively. (B) ZYG-11 negatively regulates CYB-1 levels in a proteasome-dependent manner. VSV-G–CYB-1 was coexpressed with FLAG–ZYG-11 or control FLAG–CYE-1 in HEK293T cells treated with human ZYG11A/B siRNA. Cells were treated for 8 h with nocodazole and (where indicated) the proteasome inhibitor MG132 for the last 4 h. Western blots of whole cell lysate were probed with the indicated antibodies. The relative VSV-G–CYB-1 to actin ratio is given below the top blot. Similar results were obtained in six independent experiments with varied cell treatments (± ZYG11A/B knockdown, ± nocodazole, and ± nocodazole and proTAME). (C) ZYG-11 and CYB-1 physically interact. VSV-G–CYB-1 was coexpressed in HEK293T cells with either FLAG–ZYG-11 or FLAG–CUL-4 in the presence of the proteasome inhibitor LLnL. Anti-FLAG antibody was used for IP, with analysis by Western blot (top two panels). Similar results were obtained in two independent experiments. (D) Endogenous ZYG-11 physically interacts with GFP::CYB-1 in *C. elegans*. Wild-type and animals expressing CYB-1::GFP were grown ± *cul-2* RNAi. GFP::CYB-1 was immunoprecipitated and analyzed by Western blot (top two panels). (E) ZYG-11 physically interacts with the CBOX1 domain of CYB-1. FLAG–ZYG-11 was coexpressed with VSV-G–tagged CYB-1 truncations, NTER, CBOX1, or CBOX2 in HEK293T cells in the presence of MG132. FLAG–ZYG-11 was immunoprecipitated and analyzed by Western blot (top two panels). A diagram of the full-length and truncated CYB-1 proteins is shown at bottom. The asterisk marks the location of the residue homologous to the *cyb-2.1* E120K *zyg-11* mutant suppressor allele. (F) CBOX1 of CYB-1 is degraded during meiosis in the *C. elegans* embryo in a ZYG-11–dependent manner. Bar graph showing the levels ± SEM of GFP::CYB-1 truncations in two-cell stage embryos relative to the level in meiosis I–stage embryos (set to 100) in the RNAi treatments listed; from left to right, $n = 5$, 4, 12, 4, and 7, respectively. P-values are calculated for GFP levels in two-cell stage embryos versus the corresponding meiotic embryos. For all figures, asterisks above bars represent p-values relative to the control sample; asterisks above lines denote comparisons under the lines. ns, not significant; *, $P < 0.05$; **, $P < 0.01$.

CYB-1 or if it facilitated other E3 degradation pathways, most pertinently APC/C, which also is required for the degradation of CYB-1 in the early embryo (Liu et al., 2004).

Previously, we observed that *zyg-11* RNAi stabilized the level of GFP::CYB-1 to a greater extent than RNAi of *mat-3* (the APC8/Cdc23 orthologue; Liu et al., 2004). If ZYG-11 and APC/C work in separate pathways, then inactivating both components would be expected to further stabilize GFP::CYB-1. Consistent with this, *mat-3* RNAi increased the level and stabilization of GFP::CYB-1 in *zyg-11(ts)* mutants (Fig. S1).

We have previously shown that when *C. elegans* CRL2 substrate receptors are expressed in human HEK293T cells, they form active CRL2 complexes (Starostina et al., 2007). We tested if the coexpression of ZYG-11 with CYB-1 in mammalian cells would negatively regulate CYB-1 levels and whether this regulation could be abrogated by a proteasome inhibitor. Because proteasome inhibitors arrest cells in mitosis (Giménez-Abián et al., 2005), we incubated all cells in nocodazole to ensure that an equivalent percentage of cells would be in mitosis irrespective of whether proteasome inhibitor was added. To avoid issues of redundancy, we also treated the cells with siRNA for the human ZYG-11 orthologues. We observed that coexpression of FLAG-tagged ZYG-11 with glycoprotein of vesicular stomatitis virus (VSV-G)–tagged CYB-1 in HEK293T cells resulted in an ∼50% decrease in the level of VSV-G–CYB-1 (Fig. 1 B). The decrease in VSV-G–CYB-1 levels was abrogated by incubation with proteasome inhibitor, suggesting that ZYG-11 negatively regulates CYB-1 levels in a proteasome-dependent manner.

If $CRL2^{ZYG-11}$ directly targets CYB-1 for degradation, then we would expect the two proteins to physically interact. We performed coimmunoprecipitation experiments with FLAG–ZYG-11 and VSV-G–CYB-1 expressed in HEK293T cells. In the presence of proteasome inhibitor, FLAG–ZYG-11 physically interacted with VSV-G–CYB-1 (Fig. 1 C).

To determine if ZYG-11 physically interacts with CYB-1 in *C. elegans*, we performed immunoprecipitation (IP) experiments in animals treated with *cul-2* RNAi. Inactivating *cul-2* stabilizes the endogenous ZYG-11 protein, presumably by preventing its autoubiquitylation (Sonneville and Gönczy, 2004). Depletion of CUL-2 would also be expected to stabilize the interaction of ZYG-11 with substrates by preventing their ubiquitin-mediated degradation. We observed that upon *cul-2* RNAi, endogenous ZYG-11 coprecipitated with GFP::CYB-1 (Fig. 1 D).

To map the region of CYB-1 that is required for physical association with ZYG-11, we used CYB-1 truncations. Cyclins have three structural domains: the N terminus, which contains the D-box degron; cyclin box (CBOX) 1, which binds Cdk1; and CBOX2 (Petri et al., 2007). Through coimmunoprecipitation studies in HEK293T cells, we observed that FLAG–ZYG-11 interacts with the CBOX1 domain, but not with the N-terminus or CBOX2 (Fig. 1 E).

To analyze the stability of the three regions of CYB-1 during *C. elegans* meiosis, we expressed the N terminus, CBOX1, and CBOX2 fused to GFP using the *pie-1* promoter to drive expression in the germline. We observed that the levels of CBOX1 decreased significantly during meiosis, whereas the N terminus and CBOX2 truncations were stable, suggesting that CBOX1 contains a degron (Fig. 1 F). The instability of CBOX1 during meiosis depended on the presence of ZYG-11, as *zyg-11* RNAi stabilized the CBOX1 truncation (Fig. 1 F). CBOX1 was also stabilized to a lesser extent by *mat-3* RNAi (Fig. 1 F). The finding that *mat-3* RNAi also stabilized the CBOX1 truncation could reflect a conservation of the interaction between mammalian APC/C and cyclin B1–Cdk1. In mammalian cells, APC/C physically associates with cyclin B1 predominantly via APC/C binding Cks1, which binds Cdk1 that is bound to the CBOX1 domain of cyclin B1 (van Zon et al., 2010).

### $CRL2^{ZYG11}$-mediated degradation of cyclin B1 is conserved in human cells

To determine if the $CRL2^{ZYG-11}$ pathway for cyclin B1 degradation is conserved in humans, we tested for the interaction of human ZYG11B with cyclin B1. We observed that FLAG-tagged ZYG11B coimmunoprecipitated with endogenous cyclin B1 in HEK293T cells, indicating physical interaction (Fig. 2 A). The $CRL2^{FLAG-ZYG11B}$ complex was able to ubiquitylate cyclin B1 in vitro, suggesting that cyclin B1 is a direct ubiquitylation target (Fig. 2 B).

To study the endogenous ZYG11A and ZYG11B proteins, we produced antibodies against a C-terminal ZYG11B peptide and an N-terminal ZYG11A peptide in chickens. After affinity purification, the antibodies specifically recognized the corresponding overexpressed FLAG-ZYG11A or FLAG-ZYG11B proteins in HEK293T whole cell lysates (Fig. 2 C). The two antibodies could not be used to detect endogenous ZYG11A and ZYG11B proteins in Western blots of whole cell lysate because of an excessive detection of nonspecific bands (unpublished data). However, if the antibodies were first used for IP followed by Western blotting, the endogenous ZYG11A and ZYG11B proteins could be detected (confirmed by siRNA knockdown as shown in Fig. 3 B; Fig. 2 D).

We observed that IP of endogenous cyclin B1 from HeLa cells and HEK293T cells treated with the proteasome inhibitor MG132 coprecipitated substantially more endogenous ZYG11B than a control IP with an equivalent amount of anti–VSV-G epitope antibody, suggesting that the two endogenous proteins physically associate in vivo (Fig. 2 E).

To assess the function of the human ZYG-11 orthologues, siRNA was used to knockdown ZYG11A and ZYG11B. We tested the efficiency of siRNA knockdown on transiently expressed FLAG-ZYG11A and FLAG-ZYG11B proteins in U2OS cells and found that the respective single (ZYG11A or ZYG11B) or double (ZYG11A/B) knockdowns were effective (Fig. 3 A). For endogenous ZYG11B protein, we observed effective knockdown with both ZYG11B and ZYG11A/B siRNAs and no appreciable effect from ZYG11A siRNA (Fig. 3 B). For endogenous ZYG11A protein, both ZYG11A and ZYG11A/B siRNA produced substantial knockdowns; however, ZYG11B siRNA also produced a substantial knockdown (Fig. 3 B). It is unknown whether the latter effect is caused by cross-regulation or direct targeting by siRNA.

To determine if human ZYG11A and ZYG11B contribute to the degradation of cyclin B1 independently of APC/C in mitosis, the level of cyclin B1 was analyzed in U2OS cells treated with siRNA for ZYG11A, ZYG11B, both ZYG11A and -B, or control siRNA for GFP. The cells were arrested in $G_2$ phase using the Cdk inhibitor RO-3306 (Vassilev et al., 2006). Cells were released from the $G_2$ arrest and allowed to progress into mitosis in the presence or absence of the APC/C inhibitor proTAME (Zeng et al., 2010). Endogenous cyclin B1 levels were analyzed by immunofluorescence with anti–cyclin B1 antibody. In the absence of proTAME, endogenous cyclin B1 levels were not significantly different in prometaphase and metaphase with

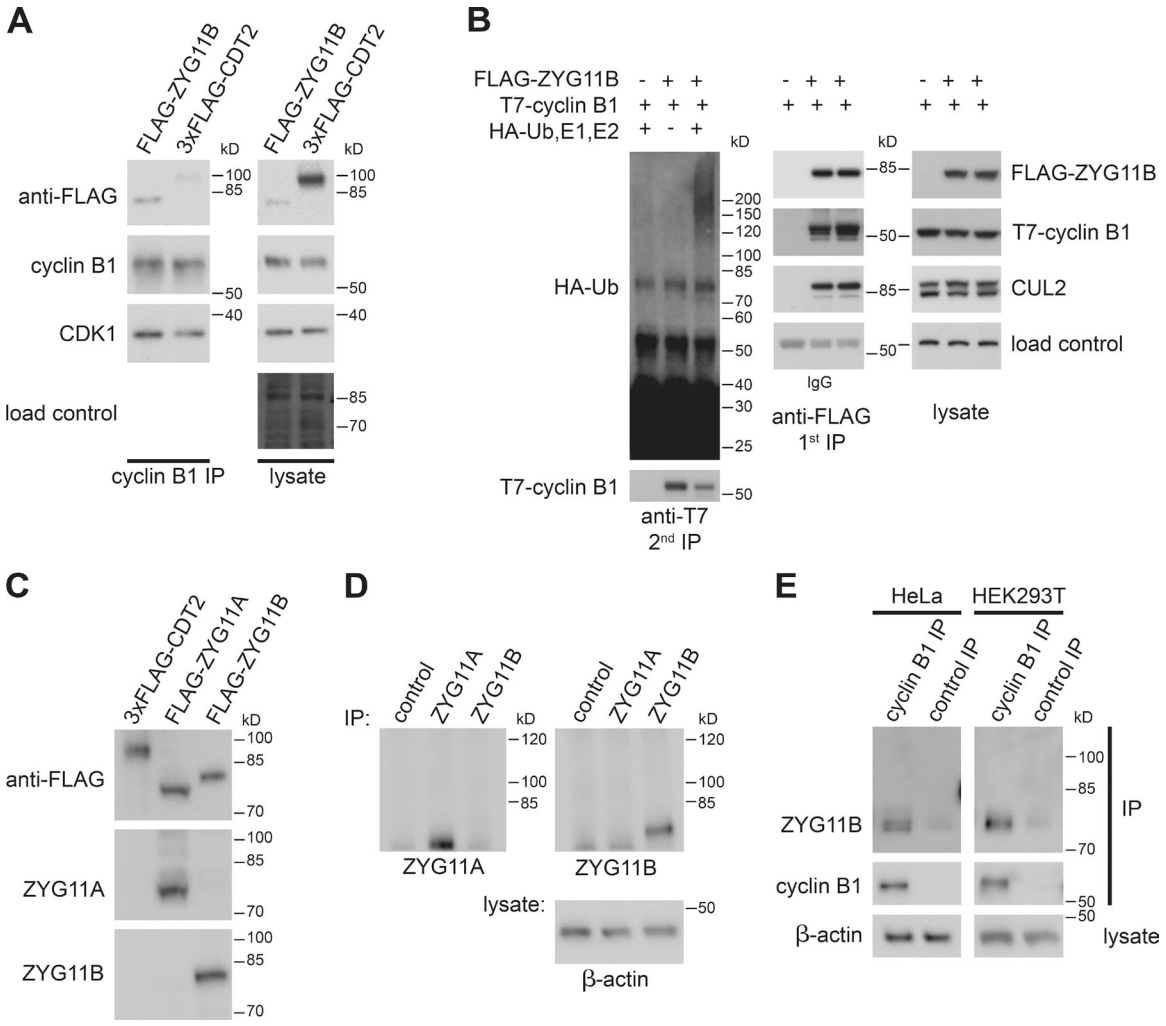


Figure 2. **Human CRL2$^{ZYG11A/B}$ physically interacts with cyclin B1.** (A) IP of endogenous cyclin B1 coprecipitates FLAG-ZYG11B in HEK293T cells treated with MG132. Left panels are for cyclin B1 IP and right panels are whole cell lysate. Similar results were obtained in two independent experiments. (B) In vitro ubiquitylation of cyclin B1 by the CRL2$^{ZYG11B}$ complex. T7-tagged cyclin B1 and FLAG-ZYG11B were coexpressed in HEK293T cells in the presence of MG132. The CRL2$^{ZYG11B}$ complex was immunoprecipitated with anti-FLAG antibody (1st IP). The immunocomplex (with associated T7–cyclin B1) was used in an in vitro ubiquitylation reaction with HA-tagged ubiquitin (Ub). T7–cyclin B1 was subsequently immunoprecipitated in the presence of 0.1% SDS (2nd IP), followed by immunoblotting for HA-ubiquitin and T7–cyclin B1. Similar results were obtained in two independent experiments. (C) Western blot showing specificity of anti-ZYG11A and anti-ZYG11B antibodies on whole cell lysate from HEK293T cells overexpressing FLAG-CDT2, FLAG-ZYG11A, or FLAG-ZYG11B. Similar results were obtained in three independent experiments. (D) IP/Western blot with control, anti-ZYG11A, and anti-ZYG11B antibodies in U2OS cells. Gels were cut above the chicken IgY antibody heavy chain band. Similar results were obtained in two independent experiments. (E) IP of endogenous cyclin B1 coprecipitates endogenous ZYG11B in HeLa and HEK293T cells treated with MG132. Control (anti–VSV-G) and anti–cyclin B1 IPs were performed from the same initial cell lysate. Similar results were obtained in three to four independent experiments.

ZYG11A, -B, or -A/B siRNA treatments compared with control GFP siRNA (unpublished data). For all siRNA treatments, endogenous cyclin B1 levels decreased at metaphase, and cells in anaphase lacked detectable cyclin B1 signal (unpublished data), consistent with previous observations (Pines and Hunter, 1991). This suggests that knockdown of ZYG11A and -B alone does not block cyclin B1 degradation during mitosis. In the presence of proTAME, the U2OS cells arrested in metaphase, as previously reported (Zeng et al., 2010). In the proTAME-arrested cells, knockdown of ZYG11A and/or -B significantly increased the levels of endogenous cyclin B1 (Fig. 3, C and D). At 2 h after $G_2$ release, cyclin B1 levels were significantly higher in ZYG11A, ZYG11B, and ZYG11A/B knockdown cells compared with control knockdown cells. In the 2-h arrested metaphase cells, cyclin B levels were increased approximately threefold with ZYG11A or ZYG11B siRNA and approximately twofold with ZYG11A/B siRNA (Fig. 3 D). In contrast to the levels in the metaphase-arrested cells, the levels of cyclin B1 in proTAME-treated cells as they entered prometaphase were only modestly higher for ZYG11A, ZYG11B, or ZYG11A/B knockdown cells compared with control knockdown cells (140 ± 14, 121 ± 10, 125 ± 15, and 100 ± 18, respectively).

It was reported that during metaphase in HeLa cells, GFP::cyclin B1 is initially lost from the spindle and chromosomes before the degradation of the cytoplasmic pool (Clute and Pines, 1999). In U2OS control knockdown cells released from RO-3306 in the absence of proTAME, we did not observe differential loss of endogenous cyclin B1 but instead observed a coordinate decrease from chromosomes, the spindle, and cytoplasm (unpublished data). However, in control knockdown cells that were treated with proTAME and arrested in metaphase, we observed that chromosome-associated cyclin

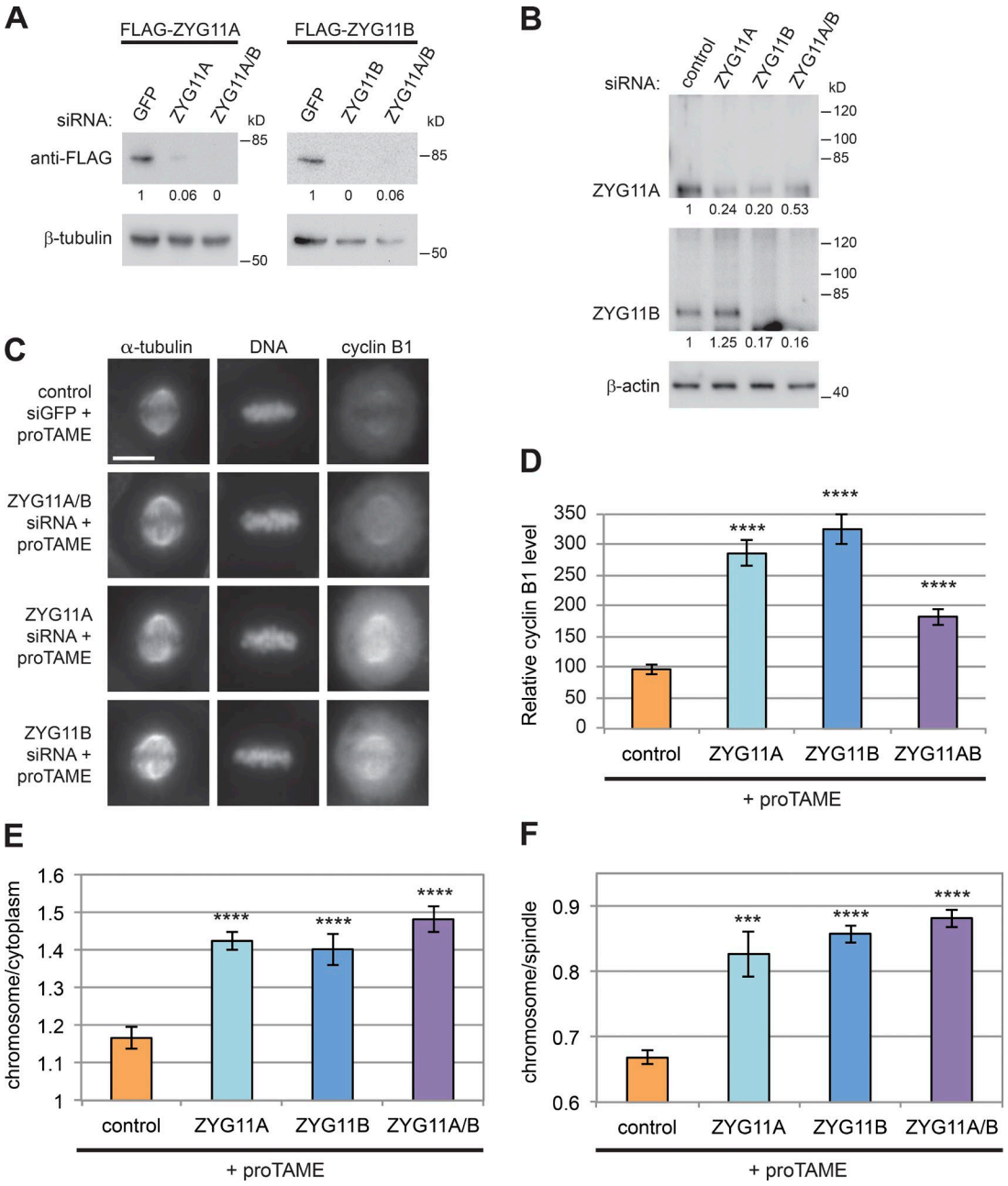


Figure 3. **Human CRL2$^{ZYG11A/B}$ negatively regulates the level of cyclin B1 in mitosis.** (A) Western blot demonstrating the effectiveness of ZYG11A and ZYG11B siRNA knockdown of FLAG-ZYG11A and FLAG-ZYG11B expressed in U2OS cells. The relative FLAG-ZYG11A/B to actin ratio is given below the blots. Similar results were obtained in two independent experiments. (B) IP/Western blot with anti-ZYG11A and anti-ZYG11B antibodies demonstrating the effectiveness of the siRNA knockdown of the endogenous proteins in U2OS cells. The relative ZYG11A/B to actin ratio is given below the blots. Comparable RNAi knockdowns were also observed in HEK293T cells (not depicted). (C) ZYG11A, ZYG11B, or ZYG11A/B siRNA knockdowns increase the level of endogenous cyclin B1 in cells treated with proTAME at 2 h after release from RO-3306 $G_2$ arrest. Epifluorescence images of representative β-tubulin, DNA, and endogenous cyclin B1 staining of metaphase-arrested proTAME-treated cells. Bar, 10 µm. (D) Bar graph shows the relative level of cyclin B1 ± SEM in the indicated siRNA treatments; *n* = 20 cells for each condition. Bar graphs presenting the ratios of the chromosome-to-cytoplasm (E) and chromosome-to-spindle (F) immunofluorescence signals ± SEM for endogenous cyclin B1 for the experiment described in C; *n* = 25 cells for each condition. For C–F, similar results were obtained in two independent experiments. ***, P < 0.001; ****, P <0.0001.

B1 levels were significantly lower relative to the surrounding cytoplasm of the spindle midzone, suggesting that cyclin B1 was preferentially depleted from the chromosomes (Fig. 3 C). The relative reduction of chromosome-localized cyclin B1 was abolished by ZYG11A, ZYG11B, and ZYG11A/B knockdowns with proTAME treatment, which had significantly higher chromosome-to-spindle and chromosome-to-cytoplasm ratios for cyclin B1 (Fig. 3, C, E, and F; and Fig. S3 A). In contrast, the spindle-to-cytoplasm ratio for cyclin B1 was not significantly different between ZYG11A/B and control knockdowns (Fig. S3 B). This suggests that although CRL2$^{ZYG11A/B}$ negatively regulates the overall level of cyclin B1 in cells in which APC/C is inhibited, it has a larger effect on chromosome-localized cyclin B1. Overall, these results suggest that human ZYG11A and ZYG11B contribute to the degradation of cyclin B1 during mitosis in a pathway that is independent of APC/C.

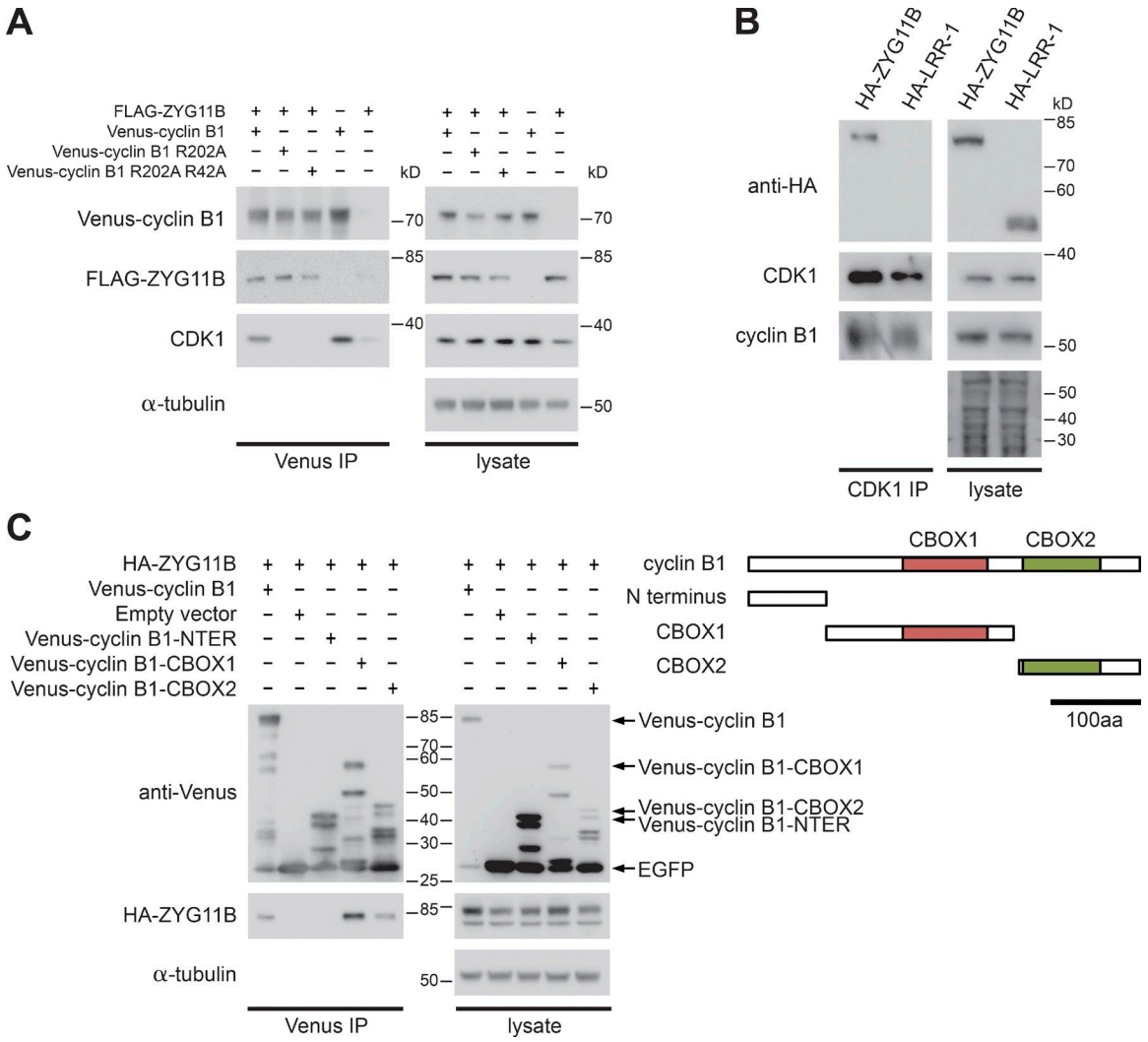


Figure 4. **Human CRL2$^{ZYG11B}$ interacts with cyclin B1 independently of Cdk1.** (A) FLAG-ZYG11B interacts with Venus–cyclin B1 mutant proteins that are incapable of binding Cdk1. FLAG-ZYG11B was coexpressed with wild-type or mutated versions of Venus–cyclin B1 with R202A or R202A R42A substitutions in HEK293T cells that were treated with MG132. The Venus tag was immunoprecipitated and immunoblotted for Venus–cyclin B1, FLAG-ZYG11B, or Cdk1 (left). Similar results were obtained in two independent experiments. (B) Endogenous Cdk1 coprecipitates HA-ZYG11B but not control HA–leucine-rich repeat (LRR) 1 in HEK293T cells treated with MG132. Similar results were obtained in two independent experiments. (C) HA-ZYG11B predominantly interacts with the CBOX1 domain of cyclin B1. HA-ZYG11B was coexpressed with Venus–cyclin B1, Venus-tagged truncations of cyclin B1 (N terminus, CBOX1, or CBOX2), or pEGFP-N1 control vector in HEK293T cells treated with MG132. Note that the truncations were cleaved into smaller isoforms in vivo (the full-length size is marked by an arrow on the right side). The Venus tag was immunoprecipitated and immunoblotted for HA or Venus tags (left panels). The results are representative of five independent experiments.

The subcellular localization of FLAG-ZYG11B is predominantly cytoplasmic during interphase and mitosis with notably less staining of interphase nuclei or condensed mitotic chromosomes (Fig. S2).

## CRL2$^{ZYG11B}$ binds cyclin B1 independently of Cdk1

The physical interaction of cyclin B1 with APC/C in human cells occurs largely through cyclin B1's interaction with Cdk1 (van Zon et al., 2010). We sought to determine if ZYG11B binding to cyclin B1 was similarly dependent on its interaction with Cdk1. ZYG11B was coexpressed with wild-type Venus–cyclin B1 or Venus–cyclin B1 with a mutation (R202A) that disrupts Cdk1 binding or a double mutation of R202A with a mutation (R42A) in the D-box that disrupts the binding of the APC/C-activating subunit Cdc20 (van Zon et al., 2010). We observed that ZYG11B bound to R202A as well as R42A, R202A-mutated Venus–cyclin B1 proteins (Fig. 4 A). This suggests that ZYG11B can bind cyclin B1 that is not associated with Cdk1. The results imply that the binding is independent of APC/C, which interacts with cyclin B1 through the D-box and via interaction with Cks1–Cdk1. Cdk1 IP coprecipitates HA-ZYG11B, suggesting that ZYG11B can physically associate with the cyclin B1–Cdk1 complex in cells (Fig. 4 B). Truncations of cyclin B1 show that, as in *C. elegans*, ZYG11B interacts with the CBOX1 region of cyclin B1, with additional interaction observed with CBOX2 (Fig. 4 C).

## CRL2$^{ZYG11A/B}$ is required for mitotic progression when cyclin B1 is overexpressed

The degradation of cyclin B1 is required for the metaphase-to-anaphase transition of mitosis. To determine whether ZYG11A/B is important for mitotic progression, we made time-lapse videos of U2OS cells after ZYG11A, ZYG11B,

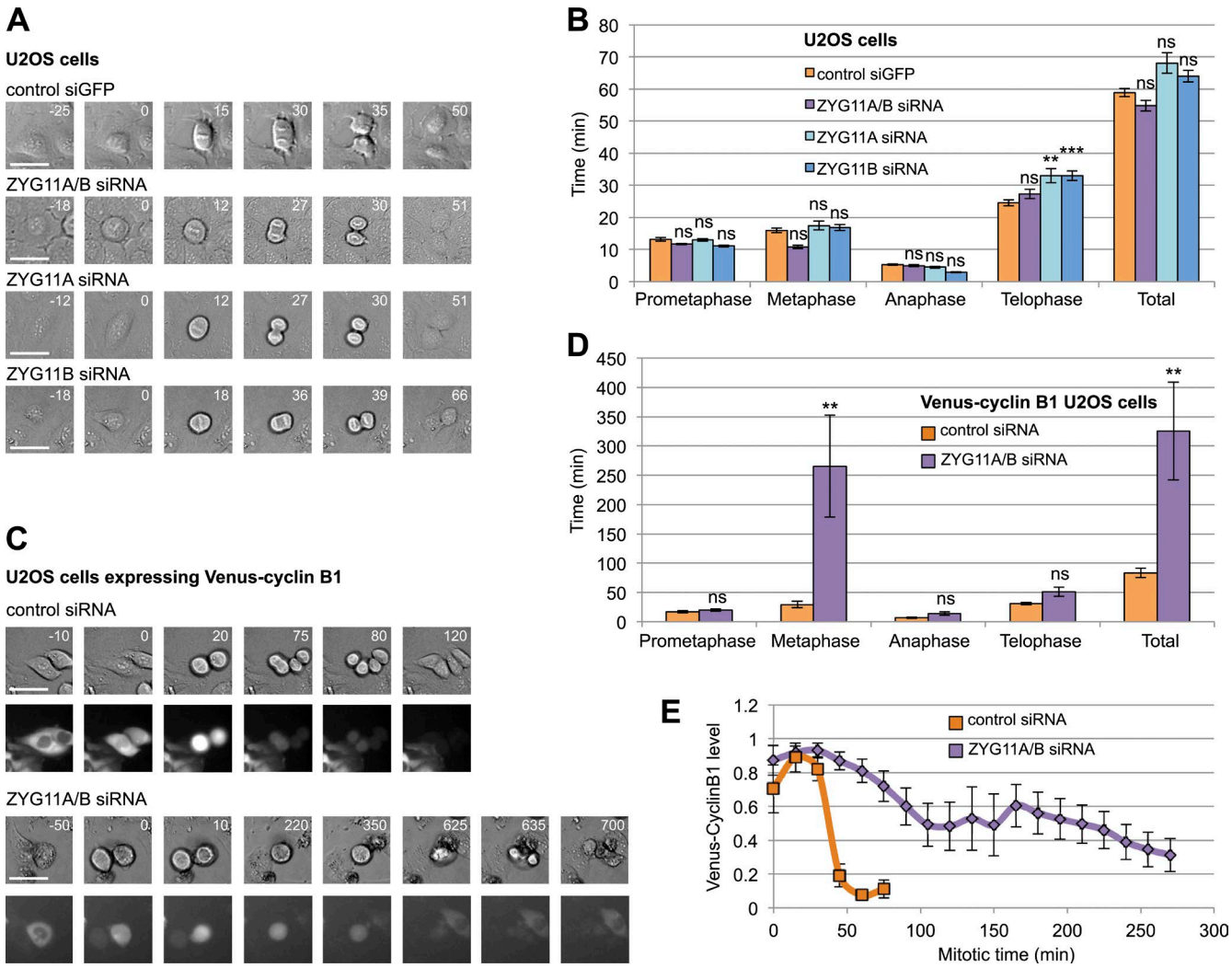


Figure 5. **Human CRL2$^{ZYG11A/B}$ is required for mitotic progression in cells overexpressing cyclin B1.** (A) DIC micrographs of U2OS cells treated with the indicated siRNAs as they progress through mitosis. Timing in minutes is shown in the top right corner of images; the 0 time point denotes nuclear envelope breakdown. The last time point reflects mitotic exit. Bars, 20 µm. (B) Bar graph of mitotic timing ± SEM for siRNA-treated U2OS cells. Timing data from two to four independent experiments are summarized in the graph; for the conditions listed from top to bottom, $n$ = 19, 18, 22, and 29, respectively. (C) Matching DIC and epifluorescence micrographs of U2OS cells expressing Venus–cyclin B1 treated with control and ZYG11A/B siRNA. (D) Bar graph of mitotic timing ± SEM for siRNA-treated U2OS cells expressing Venus–cyclin B1. Timing from three independent experiments are summarized in the graph; for conditions listed from top to bottom, $n$ = 6 and 8, respectively. Bars, 20 µm. (E) Line graph of the level of Venus–cyclin B1 in cells as they progress through mitosis (times are after nuclear envelope breakdown); $n$ = 6 and 8, as described in D. **, P < 0.01; ***, P < 0.001.

and ZYG11A/B knockdowns. We observed that the overall mitotic timing was not significantly different between the control GFP siRNA- and ZYG11 siRNA-treated cells (Fig. 5, A and B). When analyzing individual stages of mitosis, we observed a modest, but statistically significant, increase in telophase timing with ZYG11A or ZYG11B knockdowns relative to control knockdown (increasing from 24.5 ± 0.9 min to 33.1 ± 2.2 and 33.1 ± 1.5 min, respectively; Fig. 5 B). These results suggest that although ZYG11A and -B have a modest role in telophase timing, they are otherwise not essential for mitotic progression in U2OS cells under normal conditions.

To follow cyclin B1 degradation as cells progress through mitosis, we created stable U2OS cell lines expressing Venus–cyclin B1 and analyzed mitotic timing with ZYG11A/B knockdown. We observed that knockdown of ZYG11A/B significantly extended total mitotic timing relative to control knockdown in cells expressing Venus–cyclin B1 because of an extensive increase in the length of metaphase (Fig. 5, C and D). The rate of Venus–cyclin B1 degradation is substantially slower in ZYG11A/B knockdown cells compared with control knockdown cells (Fig. 5 E). These results suggest that ZYG11A/B becomes essential for normal mitotic progression when the level of cyclin B1 is elevated. The overall level of Venus–cyclin B1 for the population of cells was a mean of 46 ± 21% of the endogenous level, as determined by Western blotting with anti–cyclin B1 antibody, although the level of Venus–cyclin B1 varied significantly between cells (unpublished data).

## CRL2$^{ZYG11A/B}$ acts redundantly with APC/C to promote mitotic progression

We next asked how important ZYG11A and ZYG11B are for mitotic progression when APC/C is inhibited with proTAME. Although treatment with proTAME has been shown to generate extensive mitotic arrest and cell death in other cell lines,

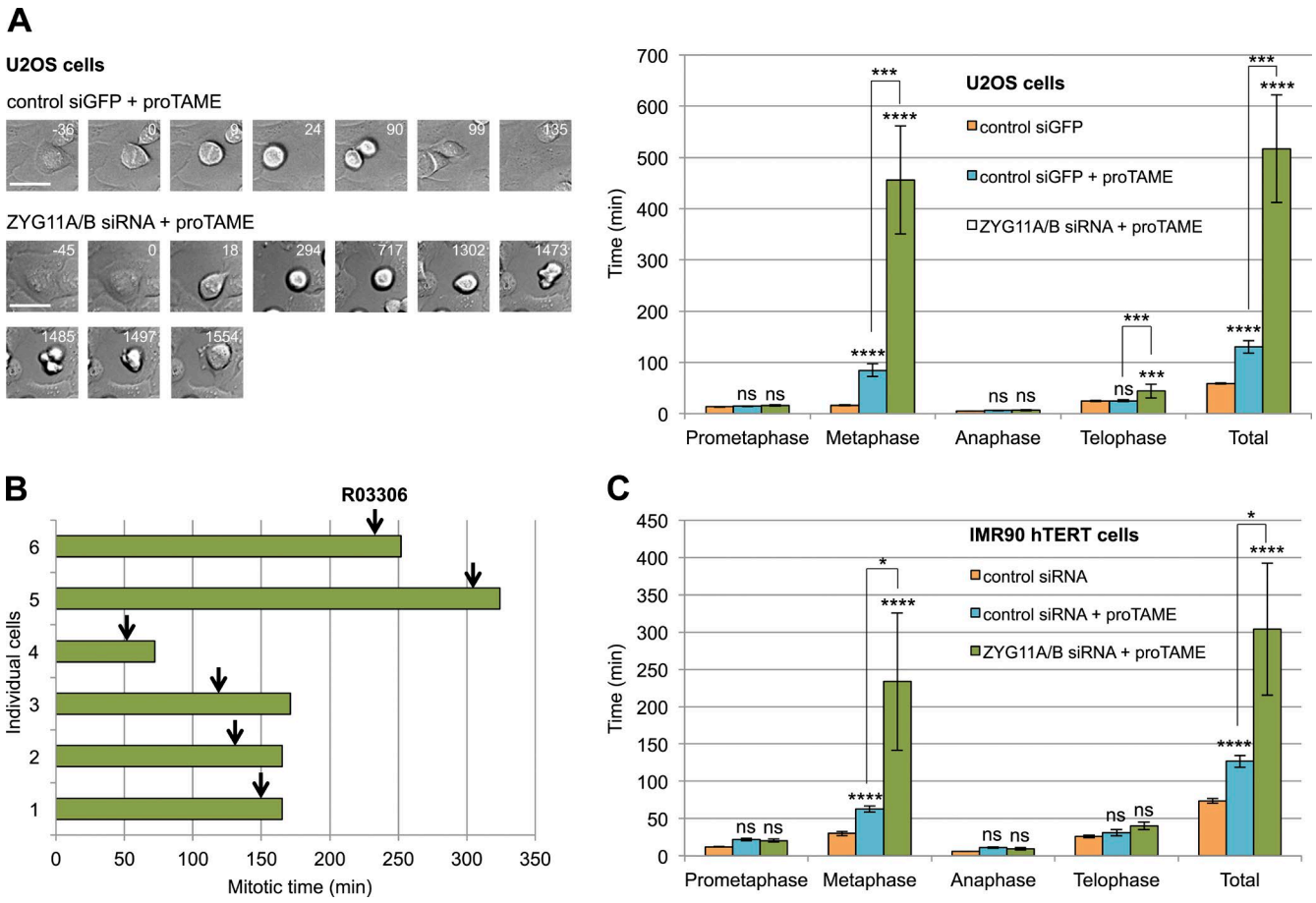


Figure 6. **Human CRL2$^{ZYG11A/B}$ functions redundantly with APC/C to promote mitotic progression.** (A) DIC micrographs of U2OS cells treated with the indicated siRNA and proTAME as they progress through mitosis. Bars, 20 µm. Bar graph of mitotic timing ± SEM for U2OS cells treated with the indicated siRNA in the presence of proTAME. The timing of control siGFP without proTAME is from Fig. 4 B and presented in the figure for comparison. The timings are from four independent experiments: control siRNA + proTAME, *n* = 23; and ZYG11A/B siRNA + proTAME, *n* = 25. (B) Inhibition of Cdk1 activity by the addition of the Cdk-inhibitor RO-3306 (arrows) allows mitotic exit. Data from three independent experiments are shown. (C) Bar graph of mitotic timing ± SEM for IMR90-hTERT cells treated with the indicated siRNA in the presence of proTAME. The timings are from two to three independent experiments; for conditions listed from top to bottom, *n* = 12, 13, and 10, respectively. *, P < 0.05; ***, P < 0.001; ****, P < 0.0001.

the reported phenotype of proTAME treatment in U2OS cells is less severe (Sackton et al., 2014). We observed that 12 µM proTAME treatment increased the total time in mitosis for U2OS control knockdown cells from 59 ± 1.3 to 130 ± 12 min, with a significant increase in the time cells spent in metaphase (16 ± 0.7 to 84 ± 12 min, a 5.25-fold increase; Fig. 6 A). This increase in mitotic timing with 12 µM proTAME is comparable to that reported previously for U2OS cells (Sackton et al., 2014). Significantly, combining proTAME with ZYG11A/B knockdown extended total mitotic timing to 517 ± 105 min, with the majority of the increase occurring in metaphase, which was extended to 455 ± 105 min (Fig. 6 A and Videos 1, 2, 3, and 4). Therefore, combining ZYG11A/B knockdown with proTAME increased metaphase timing 5.4-fold relative to control knockdown with proTAME. Although telophase timing was not significantly different in proTAME-treated control knockdown cells (24.8 ± 1.8 min) relative to untreated control knockdown cells (24.5 ± 0.9 min), we observed a 1.8-fold increase in telophase length in proTAME-treated ZYG11A/B knockdown cells (44.3 ± 13.7 min). Other stages of mitosis were not significantly different between the ZYG11A/B and control knockdowns with proTAME. 32% (8 of 25) of the ZYG11A/B knockdown plus proTAME cells underwent cell death during mitosis. These results imply that when APC/C activity is inhibited, CRL2$^{ZYG11A/B}$ becomes critical for progression through metaphase.

If the mitotic arrest upon inactivating CRL2$^{ZYG11A/B}$ and APC/C is a result of the perdurance of cyclin B1–Cdk1 activity, then inactivating Cdk1 should allow cells to exit mitosis. To test this, we added the Cdk inhibitor RO-3306 to U2OS cells arrested at metaphase with proTAME and ZYG11A/B siRNA treatment. We observed that the arrested cells exited mitosis shortly after adding the Cdk inhibitor, 23.5 ± 6.3 min after addition (Fig. 6 B). This suggests that the mitotic arrest that occurs upon inactivating APC/C and ZYG11A/B arises from the inability to inactivate cyclin B1–Cdk1.

We wanted to determine if the role of ZYG11A/B in promoting mitosis when APC/C is inhibited extended to noncancerous cells. We analyzed the effect of proTAME with or without ZYG11A/B knockdown in the human diploid embryonic lung fibroblast cell line IMR90-hTERT (Ouellette et al., 1999). The mitotic timing was increased 1.7-fold when control knockdown cells were treated with proTAME. Compared with control siRNA plus proTAME, ZYG11A/B siRNA plus proTAME increased total mitotic timing and metaphase arrest by 2.4- and 3.7-fold, respectively (127 ± 8.2 vs. 304 ± 89 and 63 ± 4.1 vs. 234 ± 92, respectively; Fig. 6 C).

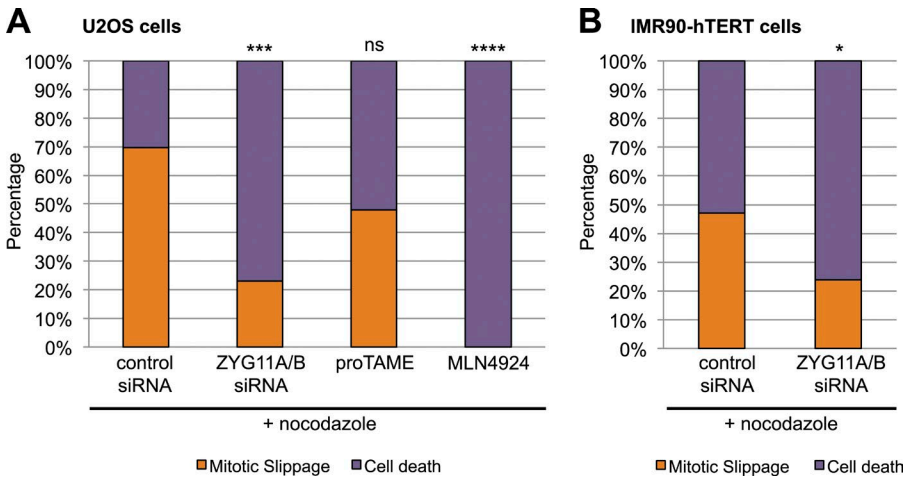


Figure 7. **Inactivation of ZYG11A/B blocks mitotic slippage in nocodazole-treated cells.** U2OS (A) and IMR90-hTERT (B) cells were treated with nocodazole under the conditions listed. Bar graphs represent the percentage of cells that underwent mitotic slippage or cell death. The $\chi^2$ significance for the occurrence of mitotic slippage is relative to nocodazole + control siRNA. The graphs summarize the data from two to four independent experiments for each condition. From left to right: for A, $n$ = 33, 39, 27, and 22; and for B, $n$ = 17 and 25, respectively. *, $P < 0.05$; ***, $P < 0.001$; ****, $P < 0.0001$.

### CRL2$^{ZYG11A/B}$ mediates mitotic slippage in mammalian cells

Mitotic slippage occurs when cells that are arrested in mitosis because of activation of the SAC exit from mitosis without cell division. It has been shown that mitotic slippage arises from the continued degradation of cyclin B1 despite an active SAC that inhibits APC/C (Brito and Rieder, 2006). The observation that ZYG11A/B contributes to cyclin B1 degradation when APC/C activity is inhibited suggested the possibility that ZYG11A/B facilitates mitotic slippage.

To determine if ZYG11A/B contributes to mitotic slippage, we analyzed the effect of ZYG11A/B knockdown on the rate of mitotic slippage in nocodazole-arrested cells. The microtubule-depolymerizing drug nocodazole blocks the formation of the mitotic spindle, resulting in the activation of the SAC. We observed that 69.7% of U2OS cells treated with control siRNA and nocodazole slipped out of mitosis. In contrast, only 21% of cells treated with ZYG11A/B siRNA and nocodazole slipped out of mitosis, indicating that ZYG11A/B acts to promote mitotic slippage (Fig. 7 A and Fig. S4 A). It has been suggested that mitotic slippage is promoted by residual APC/C activity (Lee et al., 2010), however, the addition of proTAME to the nocodazole-treated control siRNA produced only a modest (nonsignificant) reduction in mitotic slippage (Fig. 7 A and Fig. S4 A).

As an alternative method to inactivate CRL2$^{ZYG11A/B}$, we tested the effect of the small-molecule inhibitor MLN4924. MLN4924 inhibits the Nedd8-activating enzyme, which leads to the inhibition of a broad range of CRL complexes (Soucy et al., 2009). Treatment with MLN4924 would be expected to inhibit CRL2$^{ZYG11A/B}$ along with other CRL complexes. MLN4924 treatment alone did not have an appreciable effect on mitotic progression in U2OS cells, with a mean overall mitotic timing of 59.4 ± 2.2 min ($n$ = 39 cells from three independent experiments), which was similar to control and ZYG11A/B treatments. However, when MLN4924 treatment was combined with nocodazole treatment, the block on mitotic slippage was complete, and all of the mitotically arrested cells underwent cell death (Fig. 7 A and Fig. S4 A).

To determine if ZYG11A/B promotes mitotic slippage in normal cells, we analyzed IMR90-hTERT cells. We observed that the percentage of cells that undergo mitotic slippage in nocodazole-treated IMR90-hTERT cells also decreased significantly upon ZYG11A/B knockdown (24% slippage for ZYG11A/B knockdown vs. 44% slippage for control knockdown; Fig. 7 B and Fig. S4 B).

## Discussion

In this work, we show that the CRL2$^{ZYG-11}$ ubiquitin ligase complex targets cyclin B1 for degradation in a pathway that is conserved in *C. elegans* and humans. In *C. elegans*, CRL2$^{ZYG-11}$ functions redundantly with APC/C to target the degradation of maternally provided CYB-1 during the meiotic divisions. The failure to degrade CYB-1 in *zyg-11* mutants contributes to the meiosis II mutant phenotype observed in *zyg-11* mutants, as broadly lowering CYB-1 levels with RNAi against *cyb-1* or *cyb-2.1/2.2* can suppress the *zyg-11* mutant phenotype. In human cells, the two ZYG-11 orthologues ZYG11A and ZYG11B negatively regulate cyclin B1 redundantly with APC/C. CRL2$^{ZYG11A/B}$ functions independently of APC/C, as ZYG11A/B negatively regulates cyclin B1 levels when APC/C is inactivated, and ZYG11B binds to cyclin B1 through a Cdk1-independent mechanism that is distinct from APC/C binding to cyclin B1.

Inactivating ZYG11A/B does not significantly alter the timing of mitosis in otherwise unperturbed U2OS cells. However, inactivating ZYG11A/B in U2OS cells that overexpress Venus–cyclin B1 or that lack active APC/C results in severe delays in the metaphase-to-anaphase transition or cell death. ZYG11A/B also functions redundantly with APC/C to promote the metaphase-to-anaphase transition in noncancerous IMR90-hTERT cells. Our work suggests that the role of CRL2$^{ZYG11A/B}$ in degrading cyclin B1 becomes essential if cyclin B1 levels are elevated or if APC/C activity is impaired.

It has been shown in HeLa cells that GFP–cyclin B1 is initially removed from chromosomes and the spindle at the beginning of metaphase (Clute and Pines, 1999). We observed that U2OS cells arrested in metaphase with the APC/C inhibitor proTAME exhibited a differential loss of cyclin B1 on chromosomes, but not on the spindle. Knocking down ZYG11A/B in these cells restored the levels of chromosome-associated cyclin B1, suggesting that chromosome-localized cyclin B1 is particularly susceptible to negative regulation by CRL2$^{ZYG11A/B}$.

Relatively few E3s have been shown to target cyclin B1 independently of APC/C. In human cells, the ubiquitin ligase BRCA1 ubiquitylates cyclin B1 in response to DNA damage to enhance the $G_2$/M checkpoint in response to DNA damage (Shabbeer et al., 2013). In *C. elegans*, the HECT E3 ETC-1 degrades cytoplasmic GFP::cyclin B1 during meiosis redundantly with APC/C and CRL2$^{ZYG-11}$ (Wang et al., 2013). However, unlike APC/C and CRL2$^{ZYG-11}$, inactivation of ETC-1 has no effect

on viability in a wild-type background (Liu et al., 2004; Sonneville and Gönczy, 2004; Wang et al., 2013).

A significant percentage of cells that are arrested by constitutively active SAC undergo mitotic slippage (Salmela and Kallio, 2013). Mitotic slippage occurs in response to the proteasome-dependent degradation of cyclin B1 (Brito and Rieder, 2006). Mitotic slippage has been attributed to the continued activity of APC/C in nocodazole-treated human cells (HTC116, U2OS, and A549), based on the levels of known APC/C substrates falling over time (Lee et al., 2010). Inactivation of the APC/C-activating subunits Cdh1 and Cdc20 restored the levels of several APC/C substrates in these cells; however, a significant reduction in cyclin B1 levels was still observed (Lee et al., 2010). In human RPE1 retinal epithelium cells, cyclin B1 degradation occurs despite continued activity of the SAC and the failure to activate APC/$C^{Cdh1}$, which normally becomes active at anaphase (Brito and Rieder, 2006). This suggests that an E3 other than APC/C contributes to cyclin B1 degradation to promote mitotic slippage.

We found that knockdown of ZYG11A/B significantly decreases the percentage of mitotic slippage in the presence of the microtubule-destabilizing drug nocodazole for both U2OS cancer cells and noncancerous IMR90-hTERT cells. It does not appear that residual APC/C is driving the mitotic slippage, as the addition of proTAME to nocodazole-treated cells did not significantly decrease the number of U2OS cells undergoing mitotic slippage. Inactivation of cyclin B1–Cdk1 with the small molecule inhibitor RO-3306 allowed ZYG11A/B siRNA plus proTAME-treated cells to exit mitosis, suggesting that the mitotic arrest derives principally from the failure to degrade cyclin B1. Our results suggest that $CRL2^{ZYG11A/B}$-mediated degradation of cyclin B1 facilitates mitotic slippage.

Mitotic slippage leads to the formation of tetraploid cells. Tetraploidy is often a precursor to aneuploidy and genome instability, as the tetraploid cells contain extra centrosomes that can produce multipolar spindles in subsequent mitoses that then leads to the missegregation of chromosomes (King, 2008; Storchova and Kuffer, 2008). Aneuploidy and genome instability are hallmarks of solid tumors, and tetraploidy is correlated with the initial formation of many tumors (Ganem et al., 2007). Significantly, the induction of tetraploidy by itself is sufficient to induce cancer (Ganem et al., 2007; Dewhurst and Swanton, 2015). Mitotic slippage therefore heightens the risk of cancer by producing tetraploid cells. Drugs that target microtubules are widely used in chemotherapy (Field et al., 2014).

The classes of anti-microtubule drugs include taxanes, which include the drug paclitaxel/taxol, and vinca alkaloids, which include the drugs vincristine and vinblastine (Field et al., 2014). These drugs inhibit the formation or function of the mitotic spindle, thereby activating the SAC. Mitotic cells arrested by SAC activation often die, but a percentage undergo mitotic slippage (Ganem et al., 2007). There is emerging evidence that antimicrotubule drugs kill cancer cells in interphase in addition to their role in mitosis (Komlodi-Pasztor et al., 2012; Field et al., 2014). The process of mitotic slippage therefore works at cross purposes to these drugs in two ways: by limiting cell death during mitosis and by generating tetraploid cells in normal mitotically dividing tissues, which increases the risk of new cancer formation. The observation that inactivating $CRL2^{ZYG11A/B}$ prevents mitotic slippage and increases mitotic cell death when the SAC is activated suggests that ZYG11A and ZYG11B may be useful drug targets in combination with anti-microtubule drugs. Concordantly, we found that the combination of the CRL inhibitor MLN4924 with the anti-microtubule drug nocodazole completely blocked mitotic slippage. This suggests that MLN4924 and anti-microtubule drugs may provide an effective combination cancer therapy to improve the efficiency of killing mitotic cells and reduce the risk of tetraploidy.

## Materials and methods

### *C. elegans* strains and alleles

*C. elegans* strains were cultured as described (Brenner, 1974). Strains and alleles used were: JH1498, *zyg-11(ax491ts)*; ET168, *zyg-11(ax491ts) unc-4(e120)*; ET438, *zyg-11(ax491ts)*; *ekIs2* (pPD3.01b/*cyb-1* [*unc119(+)*; P*pie-1*::GFP::CYB-1::*pie-1* 3′ UTR]); ET113, *unc-119(ed3)*; *ekIs2*; CB4856, Hawaiian *C. elegans* strain; ET340, *zyg-11(ax491ts)* outcrossed six times into the CB4856 Hawaiian background; and ET308, *zyg-11(ax491ts)*; *ek14*. *zyg-11(ts)* mutants were maintained at 15°C; all other strains were maintained at 24°C.

### Mutagenesis and identification of the chromosome IV suppressor in the *zyg-11; ek14* strain

The *zyg-11(ts)* suppressor screen was performed as follows. *zyg-11(ax491ts)* hermaphrodites were synchronized by Na-hypochlorite isolation of eggs followed by L1 larval-stage arrest in M9 buffer with 5 µg/ml cholesterol (Sulston and Hodgkin, 1988). L1-stage larvae were placed on agar plates with OP50 bacteria and grown to the L4 larval stage at 16°C. The L4 larvae were mutagenized with 0.3–1 mM *N*-ethyl-*N*-nitrosourea (De Stasio and Dorman, 2001) and grown to gravid adults. F1 embryos arrested in the L1 stage were isolated from the mutagenized gravid adults and grown on OP50 bacteria at 16°C until they were gravid adults. F2 L1 larvae were isolated from F1 gravid adults, and 25 L1 larvae were placed on 6-cm nematode growth medium plates with OP50 bacteria and incubated at the nonpermissive temperature of 25°C for 3 wk. Plates in which the animals could reproduce and clear the plate of bacteria were considered to have potential suppressors. 19 suppressors were obtained from 100,000 screened F2 progeny. Each suppressor strain was outcrossed by mating with strain ET168, *zyg-11(ax491ts) unc-4(e120)*. The *unc-4* gene is tightly linked to the *zyg-11* gene, with the two genes separated by only 1.1 genetic map units. The observation of suppression of Zyg-11 Unc animals indicated that the suppressors were extragenic.

SNP mapping was performed as briefly described in this study. The suppressor strain (which has a Bristol N2 genetic background) was crossed with strain ET340, which contains the *zyg-11(ax491ts)* allele in a Hawaiianized genetic background (crossed six times into the Hawaiian strain CB4856), and grown at 16°C. 240 F2 progeny were cloned and grown at the nonpermissive temperature of 25°C to allow F3 progeny to develop. The plates of F3 progeny were segregated to identify the 30 most "suppressed" and 30 most "nonsuppressed" plates. Animals from these plates were pooled and used to isolate DNA for SNP analysis, generally by digesting the PCR-amplified product with the restriction enzyme DraI, which would distinguish N2 from the Hawaiian strain (Davis et al., 2005). Subsequent SNP analysis was also performed with DNA from individual clones of suppressed animals to map recombination endpoints.

Whole-genome sequencing of *zyg-11(ax491ts)*; *ek14* was performed by Cofactor Genomics using the Solexa genome analyzer (Illumina) 36-bp single-end reads were obtained at 13× coverage of the *C. elegans* genome. We used three programs to analyze the sequence reads. MAQGene, MAQ, and Galign programs were individually used to align the sequence reads to the *C. elegans* genome and annotate SNPs

(Li et al., 2008; Bigelow et al., 2009; Shaham, 2009). We also aligned the sequence reads to the genome with the program Bowtie, and the graphical results were visualized with the IGV genomics viewer (Langmead et al., 2009; Robinson et al., 2011). All of these approaches identified the mutation of the *cyb-2.1* gene in the *ek14* strain (Li et al., 2008; Bigelow et al., 2009; Langmead et al., 2009; Shaham, 2009), which changes amino acid residue 120 from GAA (Glu, E) to AAA (Lys, K).

### *C. elegans* RNAi and analysis

RNAi was performed by feeding animals bacteria expressing dsRNA, as described (Feng et al., 1999; Timmons et al., 2001). In brief, 10 ml overnight cultures of *Escherichia coli* HT115 (DE3) bacteria expressing dsRNA were used to inoculate 500–1000-ml flasks of 2× YT media containing 25 µg/ml tetracycline and 100 µg/ml carbenicillin at a 1:100 dilution. When the cultures were at an optical density at 600-nm wavelength of 0.4–0.6, IPTG (Gold Biotechnology) was added to the culture to 1 mM, and the culture was grown for an additional 6 h. Bacteria were collected by centrifugation at 4,000 rpm for 30 min at 4°C and resuspended in 1/200 of the original culture volume of 2× YT and used to seed nematode growth medium plates containing 1 mM IPTG and 100 µg/ml carbenicillin. RNAi plates were then left overnight at room temperature to dry, then stored at 4°C, and used within 2 wk. Animals treated with RNAi were generally grown on RNAi bacteria from embryos and analyzed as adults.

*mat-3*, *zyg-11*, *cyb-1*, and *cyb-3* RNAi feeding bacteria were obtained from the Ahringer library (Kamath et al., 2003). The RNAi construct in the Ahringer feeding RNAi library that targets *cyb-2.1* has the potential to also target *cyb-1*, so a new *cyb-2.1* RNAi feeding vector was created that contained a *cyb-2.1* sequence that is specific for *cyb-2.1* and *cyb-2.2* but is not conserved in *cyb-1*. The *cyb-2.1* sequence was PCR amplified from the RB1 cDNA library (Barstead and Waterston, 1989) with the forward and reverse primers 5′-CGAGCTCGG CAAGATATTTATGATGC-3′ and 5′-GGGTACCCCCAAGTTTTT GCTCATTCT-3′, respectively. The resulting 455-bp *cyb-2.1* cDNA sequence was cloned into the pPD129.36 double T7 promoter RNAi vector (Timmons et al., 2001) and introduced into HT115 (DE3) bacteria. Control RNAi feeding bacteria comprised HT115 (DE3) containing the pPD129.36 vector.

The effectiveness of *mat-3* RNAi was confirmed by meiotic arrest. Inactivation of *zyg-11* was assessed by embryonic arrest. Inactivation of *cyb-1* was confirmed by the elimination of GFP::CYB-1 signal.

### Expression constructs

The genomic sequence of *C. elegans cyb-1* encoding the complete CYB-1 protein (361 aa) was cloned into the *C. elegans* expression vector pID3.01b (a gift from G.C. Seydoux, Johns Hopkins University School of Medicine, Baltimore, MD) to produce a GFP–CYB-1 fusion protein expressed from the germline-specific *pie-1* promoter. Similar expression constructs were created for CYB-1 truncations: pID3.01b/NTER (residues 1–74 of CYB-1), pID3.01b/CBOX1 (residues 75–209), and pID3.01b/CBOX2 (residues 203–361). *C. elegans cyb-1* truncations for expression in mammalian cells were cloned with C-terminal VSV-G tags into the pEGFP-N1 vector (Takara Bio Inc.), with the EGFP sequence removed: pEGFP-N1/VSV-G–NTER (residues 1–74), pEGFP-N1/VSV-G–CBOX1 (residues 75–209), and pEGFP-N1/VSV-G–CBOX2 (residues 203–361).

Human ZYG11A and ZYG11B cDNAs were not available in one contiguous full-length clone. We therefore created full-length ZYG11A and ZYG11B cDNAs by fusing together cDNA sequences (for ZYG11B) and cDNA and genomic sequences (for ZYG11A) to create cDNAs corresponding to the reference sequences NM_001004339 and NM_024646, respectively. The cDNAs were confirmed by sequencing. ZYG11A and ZYG11B were cloned into the pCMV-Tag2B expression vector (Agilent Technologies) for expression in mammalian cells as N-terminal FLAG-tagged proteins. ZYG11B was cloned into pEGFP-N1, after the EGFP sequence was removed, as an N-terminal HA-tagged protein.

pVenus-N1 cyclin B1 and pVenus–cyclin B1 (R42A) expression vectors were created by the Pines laboratory (Hagting et al., 2002) and obtained from Addgene (plasmids 26062 and 39873, respectively). pVenus-N1 cyclin B1 (R202A and R42A) was made by introducing the R202A mutation into the pVenus-N1 cyclin B1 (R42A) construct using an overlap-extension mutagenesis method (Mikaelian and Sergeant, 1992). Truncations of cyclin B1 were created in the pVenus–N1 cyclin B1 vector: pVenus–N1 cyclin B1 NTER (residues 1–86 of cyclin B1); pVenus–N1 cyclin B1 CBOX1 (residues 87–294); and pVenus–N1 cyclin B1 CBOX2 (residues 300–433). Human cyclin B1 was cloned with an N-terminal T7 tag into pEGFP-N1 with the EGFP sequence removed.

### Antibodies

We tested commercially available antibodies for ZYG11A (two antibodies) and ZYG11B (three antibodies) and found that they were unable to detect either endogenous or transiently expressed ZYG11A and ZYG11B proteins by Western blotting. ZYG11A and ZYG11B proteins are highly conserved among humans, mouse, rabbit, and goat (98 to 99% sequence identities between the orthologues), and this conservation may hinder the generation of effective antibodies in these species. Human ZYG11A and ZYG11B differ substantially from their chicken orthologues in their N and C termini.

A ZYG11A peptide near the N terminus (6–26), HPGHTPRNI VPPDAQKDALGC, and a C-terminal ZYG11B peptide (712–721), CKKQPQARLN, were synthesized by ELIM BIOPHARM for antibody production. These peptides were conjugated to maleimide-activated mariculture keyhole limpet hemocyanin (Thermo Fisher Scientific) to increase immunogenicity. The conjugated peptides were sent to GeneTel Laboratories for antibody production, where ZYG11A and ZYG11B peptides were each used to immunize two chickens. The antibodies used in the experiments were purified from the bleeds from day 35. The antibodies in the serum were affinity purified by running them through a column with the peptides linked to SulfoLink Coupling resin (Thermo Fisher Scientific), followed by an acid elution. The affinity-purified antibodies were used for Western blots at a dilution of 1:20,000 (stock concentration of 0.7 mg/ml for anti-ZYG11A and 0.9 mg/ml for anti-ZYG11A) and a concentration of 4 µg/ml for IPs.

The apparent molecular mass based on SDS-PAGE mobility for the endogenous ZYG11A (72 kD) and ZYG11B (79 kD) proteins were similar to, but slightly smaller than, the ectopic FLAG-ZYG11A (77.5 kD) and FLAG-ZYG11B (82 kD) proteins, even when considering the size of the FLAG tag. This suggests the possibility of different posttranslational modifications for the endogenous proteins or altered splicing relative to the predicted reference sequences upon which the ectopic expression constructs were designed.

The following rabbit primary antibodies were used: anti–cyclin B1 (sc-752; Santa Cruz Biotechnology, Inc.); anti-Cdk1 (EMD Millipore); anti–VSV-G (Bethyl Laboratories, Inc.); anti-T7 (D9E1X; Cell Signaling Technology); and anti–ZYG-11 (Vasudevan et al., 2007). The following mouse primary antibodies were used: anti–α-tubulin (DM1A; Sigma-Aldrich); anti–β-tubulin (D-10; Santa Cruz Biotechnology, Inc.); anti–β-actin (Bio-Rad Laboratories); anti-HA (16B12; Abcam); anti-T7 (EMD Millipore); anti-FLAG (M2; Sigma-Aldrich); anti-GFP (GF28R; Thermo Fisher Scientific); and anti–VSV-G (P5D4; Sigma-Aldrich). The following secondary antibodies were used: anti–mouse HRP (Thermo Fisher Scientific); anti–rabbit HRP (Thermo Fisher Scientific); anti–chicken HRP (Invitrogen); anti–chicken Dylight 488 (Thermo Fisher

Scientific), and anti–mouse rhodamine (Cappel Research Reagents). For IPs, protein G sepharose beads (Invitrogen) were used for rabbit and mouse antibody pulldowns, and donkey anti–chicken IgY Agarose beads (Gallus Immunotech) were used for chicken antibody pulldowns.

### Cell culture, selection, and synchronization

HEK293T and human osteosarcoma cells (U2OS) were obtained from ATCC and cultured in DMEM in the presence of 10% FBS (Sigma-Aldrich) and 100 µg/ml penicillin and streptomycin (HyClone; GE Healthcare). Cells were synchronized at S phase with a double thymidine (Sigma-Aldrich) block. The first 2.5-mM thymidine block was for 18 h, followed by a 9-h release into fresh media, and a second 2.5-mM thymidine block for 18 h. Cells arrested in $G_2$ phase were obtained by releasing cells from double thymidine block for 3 h, followed by the addition of 9 µM RO-3306 (Sigma-Aldrich), a Cdk1 inhibitor, for 8 h. Cells arrested in prometaphase and metaphase were obtained by releasing cells from a double thymidine block for 3 h, followed by either incubation with 100 ng/ml nocodazole (Sigma-Aldrich) or 12 µM proTAME (Boston Biochem), respectively, for 10 h.

### DNA transfections, siRNA knockdowns, IPs, and immunofluorescence

*C. elegans* proteins were expressed in HEK293T cells and immunoprecipitated as described (Starostina et al., 2007; Kim et al., 2008). HEK293T cells were transfected with plasmids for human protein expression with polyethylenimine (Boussif et al., 1995). U2OS cells were transfected with plasmids for protein expression using Lipofectamine 2000 (Invitrogen) according to the manufacturer's instructions. U2OS cells expressing Venus–cyclin B1 were selected after transfection with 500 µg/ml G418 (Gold Biotechnology). For IP of human proteins, proteasome inhibition treatments were for 8 h (unless otherwise noted) and used: 15 µM MG132 (Sigma-Aldrich) or 50 µM Leu-Leu-norleucinal (LLnL; Sigma-Aldrich). Cells were collected 48 h after transfection and lysed in NP-40 buffer (0.5% NP-40, 150 mM NaCl, 50 mM Tris, pH 7.4, and 1 mM EDTA), protease inhibitor cocktail (Roche), 2 mM DTT, and 50 µM LLnL. Cell lysates were centrifuged at 13,000 rpm for 25 min at 4°C, and the supernatant was precleared with sepharose 4B beads (Sigma-Aldrich). Cyclin B1 and Cdk1 antibodies were used at a concentration of 1:150 to bind endogenous proteins and captured on protein G Sepharose beads (GE Healthcare). GFP-nanoAb agarose beads (Allele Biotechnology) were used for Venus IPs according to the manufacturer's instructions.

For immunofluorescence, U2OS cells transfected with FLAG-ZYG11B were grown on eight-well Lab-Tek II chamber slides (Thermo Fisher Scientific) and fixed for 30 min at room temperature with a formaldehyde fixation mixture of 3.7% formaldehyde, 80 mM Hepes, pH 6.9, 0.8 mM EGTA, and 1.6 mM $MgSO_4$. Cells were washed three times with PBT (PBS with 0.1% Triton X-100 and 0.1% BSA) and kept in PBT overnight as a blocking solution. Primary antibodies (mouse monoclonal anti-FLAG M2, 1:650 dilution; and rabbit monoclonal anti–cyclin B1, 1:66) in PBT were incubated with the fixed cells for 2 h and then washed with PBT. Secondary antibodies (Dylite 488 anti–rabbit; 1:500; and rhodamine anti–mouse) were incubated in PBT for 30 min, washed, and mounted for viewing in 1 mg/ml *p*-phenylenediamine (antifade agent) and 90% glycerol. Images of the same antibodies/Hoechst were taken with the same exposure times and processed identically using Photoshop software (Adobe Systems). Quantitation of nuclear and total immunofluorescence signal was performed with Open*lab* software (version 5.0; PerkinElmer).

siRNA pools were transfected using RNAiMAX (Invitrogen) according to the manufacturer's instructions. siRNA transfections were performed twice, separated by an interval of 24 h. siRNA pools were purchased from Thermo Fisher Scientific as ON-TARGET pools for ZYG11A and ZYG11B. The siRNAs for ZYG11A were: 5′-CUUCCA AGCUGGUGACCGAUU-3′; 5′-GCUCACUGGUCUUCGCAUUUU-3′; 5′-GCAAACAAUGGCAGUGAGUUU-3′; 5′-CAGAAGCACUGAGCC GAUAUU-3′. The siRNAs for ZYG11B were: 5′-GGUGAUGAG AAUAGCCGUAUU-3′; 5′-GCUUGGACAUUGAGUCGUAUU-3′; 5′-GAUUAGAGAGCUUGGAUAUUU-3′; 5′-GGAAUUUGCUUU CGUGAUAUU-3′. siRNA controls were purchased from Invitrogen. Control siRNA was 5′-GUAUCUCUUCAUAGCCUUADTDT-3′ and GFP siRNA was 5′-GCUGACCCUGAAGUUCAUCUGDTDT-3′. Because we observed a reduction in ZYG11A protein with ZYG11B siRNA, it should be noted that the third-listed ZYG11B siRNA has the highest potential cross-reactivity among all of the ZYG11A/B siRNAs. At the homologous site in ZYG11A, the ZYG11B siRNA shares 6 of 7 identical residues in the seed region of the siRNA, with an overall identity of 15 of 19 residues.

For the knockdown of overexpressed proteins in U2OS cells, DNA was transfected using Lipofectamine 2000 (Invitrogen) according to the manufacturer's instructions followed by the siRNA transfections after 24 h.

### In vitro ubiquitylation assay

FLAG-ZYG11B and T7–cyclin B1 were coexpressed in HEK293T cells for 26 h, with 10 µM MG132 added for the last 6 h. Cells were lysed with NP-40 buffer: 0.5% NP-40, 50 mM Tris-HCl, pH 7.6, 150 mM NaCl, protease inhibitor cocktail, 2 mM DTT, 10% glycerol, 10 mM $MgCl_2$, 15 µM MG132, and 100 U/ml OmniCleave endonuclease (Epicentre Biotechnologies). FLAG-ZYG11B was precipitated with anti-FLAG antibody in the presence of 1 mM EDTA, 2.5 mM iodoacetamide, and 2.5 mM *O*-phenanthroline. The immunocomplex was precipitated with protein G sepharose, washed with lysis buffer, and incubated with 30 µl ubiquitylation reaction mix containing 50 mM Tris-HCl, pH 7.4, 5 mM $MgCl_2$, 2 mM NaF, 10 nM okadaic acid, 0.6 mM DTT, 2 mM ATP, 0.6 µl energy generation solution (Enzo Life Sciences), 1 µg HA-ubiquitin (Boston Biochem), 100 ng human E1 (Enzo Life Sciences), 400 ng human E2-UbcH5a (Enzo Life Sciences), 2 µM ubiquitin aldehyde (Enzo Life Sciences), and 15 µM MG132. Reactions were incubated at 30°C for 90 min and terminated by boiling with 1% SDS. T7–cyclin B1 was immunoprecipitated in a buffer containing 0.1% SDS and 50 mM Tris-HCl, pH 7.6, 150 mM NaCl, 0.1% NP-40, 2 mM DTT, 1 mM EDTA, protease inhibitor cocktail, phosphatase inhibitor cocktail, 15 µM MG132, and 5 mM iodoacetamide (Sigma-Aldrich) and analyzed by Western blot for HA-ubiquitin and T7–cyclin B1.

### Microscope image acquisition and time-lapse microscopy

Microscopy for *C. elegans* epifluorescence and human cell immunofluorescence (Figs. 1 F and 3; and Figs. S1, S2, and S3) was performed with an Axioplan microscope equipped with an LuDL hardware controller (ZEISS), automated filter wheels and shutters, and an Apple iMac computer running Open*lab* software, version 5.5.2 (PerkinElmer). Epifluorescence images were taken with a Plan-Achromat 63× Oil DIC objective (ZEISS), with an NA of 1.40 at room temperature. Images were captured with an ORCA-ER CCD camera (Hamamatsu Photonics) as 12-bit grayscale images at a resolution of 1,344 × 1,024 pixels.

For quantitation of whole cell levels of human cyclin B1 (Fig. 3 B), the signal minus background was multiplied by the pixels to determine the total signal. For the analysis of the ratios of chromosome-, spindle-, and cytoplasm-localized cyclin B1 levels (Fig. 3, C and D; and Fig. S3), the mean signal (minus background) for each subcellular compartment was compared. The following fluorochromes were used: Dylight 488, rhodamine, and Hoechst.

Time-lapse videos of *C. elegans* embryos were made of embryos in utero at 22°C. Gravid adults were treated with 10 mM levamisole

(Sigma-Aldrich) to paralyze striated muscles and mounted on slides with a 2.5% agarose pad covered with a 22 × 22-mm coverslip. Videos were made with sequential differential interference contrast (DIC) and epifluorescence images of EGFP every 60 s.

Microscopy for time-lapse videos of human cells (Figs. 4, 5, and 6) was performed with a DeltaVision Microscope System II (GE Healthcare) in a heated chamber at 37°C. The microscope was controlled by SoftWoRX software (GE Healthcare). Images were taken with a UPlanSApo 20× DIC objective with an NA of 0.75 (Olympus). DIC images were taken every 3 or 5 min using a 25-ms exposure time. Epifluorescence images of Venus–cyclin B1 were taken every 5 min using a 400-ms exposure time. Images were 16-bit grayscale at a resolution of 1024 × 1024 pixels. U2OS or IMR90-hTERT cells were plated for imaging on 35-mm glass-bottom plates (MatTek Corporation) and transfected with siRNA when 70% confluent, as described in the DNA transfection, siRNA knockdowns, IPs, and immunofluorescence section. Immediately before imaging, the medium was changed to $CO_2$-independent media (Gibco). For the mitotic arrest rescue experiment (Fig. 6 B), the cells were treated with 12 µM proTAME, and then RO-3306 was added (to 9 µM) 6 h after the start of the video. For mitotic slippage experiments, 100 µg/ml nocodazole was added to the $CO_2$-independent media, and DIC images were obtained every 3 min. A concentration of 1 µM MLN4924 (Cayman Chemical) was used to broadly inhibit CRL complexes. Images were processed with Photoshop; videos were processed with ImageJ software (National Institutes of Health; Schneider et al., 2012). Epifluorescent images for quantitative comparison were taken with the same exposure and treated identically with no gamma adjustments. Signal levels were determined using Photoshop, with the background level from the same image subtracted from the signal.

### Statistical analysis

Student's *t* test was used to determine significance for Fig. 1 (A and F) and Fig. 2 (D and E). The Mann–Whitney test was used to determine significance of mitotic timing as a result of the nonparametric nature of the data (Fig. 4, B and D; Fig. 5, A and C; and Fig. 6). The $\chi^2$ test was used to determine the significance of mitotic slippage occurrence (Fig. 7). Error bars in all figures represent SEM.

### Online supplemental material

Table S1 shows the rescue of *C. elegans zyg-11(ts)* phenotypes by *cyb-2.1/2.2* RNAi. Fig. S1 shows the increase in GFP::CYB-1 levels in *zyg-11(ts)* embryos treated with *mat-3* RNAi compared with untreated *zyg-11(ts)* embryos. Fig. S2 shows the subcellular localization of FLAG-ZYG11B during prometaphase and interphase in U2OS cells. Fig. S3 shows the relative levels of endogenous cyclin B1 on chromosomes, mitotic spindle, and cytoplasm with control, ZYG11A, ZYG11B, or ZYG11A/B siRNA treatments in the presence of proTAME. Fig. S4 shows the timing of mitotic slippage and cell death in nocodazole-treated cells. Video 1 shows mitotic progression of U2OS cells treated with control GFP siRNA. Video 2 shows mitotic progression of U2OS cells treated with ZYG11A/B siRNA. Video 3 shows mitotic progression of U2OS cells treated with siGFP and proTAME. Video 4 shows mitotic progression of U2OS cells treated with ZYG11A/B siRNA and proTAME.

## Acknowledgments

We thank G.C. Seydoux for reagents. Some strains were provided by the *Caenorhabditis* Genetics Center, which is funded by the National Institutes of Health Office of Research Infrastructure Programs (P40 OD010440).

This work was supported by the National Institute of General Medical Sciences (National Institutes of Health) grant R01 GM074212.

The authors declare no competing financial interests.

Submitted: 25 January 2016
Accepted: 22 September 2016

## References

Barstead, R.J., and R.H. Waterston. 1989. The basal component of the nematode dense-body is vinculin. *J. Biol. Chem.* 264:10177–10185.

Bigelow, H., M. Doitsidou, S. Sarin, and O. Hobert. 2009. MAQGene: software to facilitate *C. elegans* mutant genome sequence analysis. *Nat. Methods.* 6:549. http://dx.doi.org/10.1038/nmeth.f.260

Boussif, O., F. Lezoualc'h, M.A. Zanta, M.D. Mergny, D. Scherman, B. Demeneix, and J.P. Behr. 1995. A versatile vector for gene and oligonucleotide transfer into cells in culture and in vivo: polyethylenimine. *Proc. Natl. Acad. Sci. USA.* 92:7297–7301. http://dx.doi.org/10.1073/pnas.92.16.7297

Brenner, S. 1974. The genetics of *Caenorhabditis elegans*. *Genetics*. 77:71–94.

Brito, D.A., and C.L. Rieder. 2006. Mitotic checkpoint slippage in humans occurs via cyclin B destruction in the presence of an active checkpoint. *Curr. Biol.* 16:1194–1200. http://dx.doi.org/10.1016/j.cub.2006.04.043

Chang, D.C., N. Xu, and K.Q. Luo. 2003. Degradation of cyclin B is required for the onset of anaphase in Mammalian cells. *J. Biol. Chem.* 278:37865–37873. http://dx.doi.org/10.1074/jbc.M306376200

Ciosk, R., W. Zachariae, C. Michaelis, A. Shevchenko, M. Mann, and K. Nasmyth. 1998. An ESP1/PDS1 complex regulates loss of sister chromatid cohesion at the metaphase to anaphase transition in yeast. *Cell.* 93:1067–1076. http://dx.doi.org/10.1016/S0092-8674(00)81211-8

Clute, P., and J. Pines. 1999. Temporal and spatial control of cyclin B1 destruction in metaphase. *Nat. Cell Biol.* 1:82–87. http://dx.doi.org/10.1038/10049

Davis, M.W., M. Hammarlund, T. Harrach, P. Hullett, S. Olsen, and E.M. Jorgensen. 2005. Rapid single nucleotide polymorphism mapping in *C. elegans*. *BMC Genomics.* 6:118. http://dx.doi.org/10.1186/1471-2164-6-118

De Stasio, E.A., and S. Dorman. 2001. Optimization of ENU mutagenesis of *Caenorhabditis elegans*. *Mutat. Res.* 495:81–88. http://dx.doi.org/10.1016/S1383-5718(01)00198-X

Dewhurst, S., and C. Swanton. 2015. Tetraploidy and CIN: a dangerous combination. *Cell Cycle.* 14:3217. http://dx.doi.org/10.1080/15384101.2015.1084208

Deyter, G.M., T. Furuta, Y. Kurasawa, and J.M. Schumacher. 2010. *Caenorhabditis elegans* cyclin B3 is required for multiple mitotic processes including alleviation of a spindle checkpoint-dependent block in anaphase chromosome segregation. *PLoS Genet.* 6:e1001218. http://dx.doi.org/10.1371/journal.pgen.1001218

Errico, A., K. Deshmukh, Y. Tanaka, A. Pozniakovsky, and T. Hunt. 2010. Identification of substrates for cyclin dependent kinases. *Adv. Enzyme Regul.* 50:375–399. http://dx.doi.org/10.1016/j.advenzreg.2009.12.001

Feng, H., W. Zhong, G. Punkosdy, S. Gu, L. Zhou, E.K. Seabolt, and E.T. Kipreos. 1999. CUL-2 is required for the G1-to-S-phase transition and mitotic chromosome condensation in Caenorhabditis elegans. *Nat. Cell Biol.* 1:486–492. http://dx.doi.org/10.1038/70272

Field, J.J., A. Kanakkanthara, and J.H. Miller. 2014. Microtubule-targeting agents are clinically successful due to both mitotic and interphase impairment of microtubule function. *Bioorg. Med. Chem.* 22:5050–5059. http://dx.doi.org/10.1016/j.bmc.2014.02.035

Ganem, N.J., Z. Storchova, and D. Pellman. 2007. Tetraploidy, aneuploidy and cancer. *Curr. Opin. Genet. Dev.* 17:157–162. http://dx.doi.org/10.1016/j.gde.2007.02.011

Giménez-Abián, J.F., L.A. Díaz-Martínez, K.G. Wirth, C. De la Torre, and D.J. Clarke. 2005. Proteasome activity is required for centromere separation independently of securin degradation in human cells. *Cell Cycle.* 4:1558–1560. http://dx.doi.org/10.4161/cc.4.11.2145

Gorr, I.H., D. Boos, and O. Stemmann. 2005. Mutual inhibition of separase and Cdk1 by two-step complex formation. *Mol. Cell.* 19:135–141. http://dx.doi.org/10.1016/j.molcel.2005.05.022

Hagting, A., N. Den Elzen, H.C. Vodermaier, I.C. Waizenegger, J.M. Peters, and J. Pines. 2002. Human securin proteolysis is controlled by the spindle checkpoint and reveals when the APC/C switches from activation by Cdc20 to Cdh1. *J. Cell Biol.* 157:1125–1137. http://dx.doi.org/10.1083/jcb.200111001

Hauf, S., I.C. Waizenegger, and J.M. Peters. 2001. Cohesin cleavage by separase required for anaphase and cytokinesis in human cells. *Science.* 293:1320–1323. http://dx.doi.org/10.1126/science.1061376

Holloway, S.L., M. Glotzer, R.W. King, and A.W. Murray. 1993. Anaphase is initiated by proteolysis rather than by the inactivation of maturation-promoting factor. *Cell.* 73:1393–1402. http://dx.doi.org/10.1016/0092-8674(93)90364-V

Huang, X., R. Hatcher, J.P. York, and P. Zhang. 2005. Securin and separase phosphorylation act redundantly to maintain sister chromatid cohesion in mammalian cells. *Mol. Biol. Cell.* 16:4725–4732. http://dx.doi.org/10.1091/mbc.E05-03-0190

Huang, X., C.V. Andreu-Vieyra, J.P. York, R. Hatcher, T. Lu, M.M. Matzuk, and P. Zhang. 2008. Inhibitory phosphorylation of separase is essential for genome stability and viability of murine embryonic germ cells. *PLoS Biol.* 6:e15. http://dx.doi.org/10.1371/journal.pbio.0060015

Huang, X., C.V. Andreu-Vieyra, M. Wang, A.J. Cooney, M.M. Matzuk, and P. Zhang. 2009. Preimplantation mouse embryos depend on inhibitory phosphorylation of separase to prevent chromosome missegregation. *Mol. Cell. Biol.* 29:1498–1505. http://dx.doi.org/10.1128/MCB.01778-08

Jongsma, M.L., I. Berlin, and J. Neefjes. 2015. On the move: organelle dynamics during mitosis. *Trends Cell Biol.* 25:112–124. http://dx.doi.org/10.1016/j.tcb.2014.10.005

Kamath, R.S., A.G. Fraser, Y. Dong, G. Poulin, R. Durbin, M. Gotta, A. Kanapin, N. Le Bot, S. Moreno, M. Sohrmann, et al. 2003. Systematic functional analysis of the *Caenorhabditis elegans* genome using RNAi. *Nature.* 421:231–237. http://dx.doi.org/10.1038/nature01278

Kettenbach, A.N., D.K. Schweppe, B.K. Faherty, D. Pechenick, A.A. Pletnev, and S.A. Gerber. 2011. Quantitative phosphoproteomics identifies substrates and functional modules of Aurora and Polo-like kinase activities in mitotic cells. *Sci. Signal.* 4:rs5. http://dx.doi.org/10.1126/scisignal.2001497

Kim, Y., N.G. Starostina, and E.T. Kipreos. 2008. The CRL4Cdt2 ubiquitin ligase targets the degradation of p21Cip1 to control replication licensing. *Genes Dev.* 22:2507–2519. http://dx.doi.org/10.1101/gad.1703708

King, R.W. 2008. When 2+2=5: the origins and fates of aneuploid and tetraploid cells. *Biochim. Biophys. Acta.* 1786:4–14. http://dx.doi.org/10.1016/j.bbcan.2008.07.007

Komlodi-Pasztor, E., D.L. Sackett, and A.T. Fojo. 2012. Inhibitors targeting mitosis: tales of how great drugs against a promising target were brought down by a flawed rationale. *Clin. Cancer Res.* 18:51–63. http://dx.doi.org/10.1158/1078-0432.CCR-11-0999

Lancaster, O.M., and B. Baum. 2014. Shaping up to divide: coordinating actin and microtubule cytoskeletal remodelling during mitosis. *Semin. Cell Dev. Biol.* 34:109–115. http://dx.doi.org/10.1016/j.semcdb.2014.02.015

Langmead, B., C. Trapnell, M. Pop, and S.L. Salzberg. 2009. Ultrafast and memory-efficient alignment of short DNA sequences to the human genome. *Genome Biol.* 10:R25. http://dx.doi.org/10.1186/gb-2009-10-3-r25

Lee, J., J.A. Kim, R.L. Margolis, and R. Fotedar. 2010. Substrate degradation by the anaphase promoting complex occurs during mitotic slippage. *Cell Cycle.* 9:1792–1801. http://dx.doi.org/10.4161/cc.9.9.11519

Li, H., J. Ruan, and R. Durbin. 2008. Mapping short DNA sequencing reads and calling variants using mapping quality scores. *Genome Res.* 18:1851–1858. http://dx.doi.org/10.1101/gr.078212.108

Liu, J., S. Vasudevan, and E.T. Kipreos. 2004. CUL-2 and ZYG-11 promote meiotic anaphase II and the proper placement of the anterior-posterior axis in *C. elegans*. *Development.* 131:3513–3525. http://dx.doi.org/10.1242/dev.01245

Lydeard, J.R., B.A. Schulman, and J.W. Harper. 2013. Building and remodelling Cullin-RING E3 ubiquitin ligases. *EMBO Rep.* 14:1050–1061. http://dx.doi.org/10.1038/embor.2013.173

Mei, J., X. Huang, and P. Zhang. 2001. Securin is not required for cellular viability, but is required for normal growth of mouse embryonic fibroblasts. *Curr. Biol.* 11:1197–1201. http://dx.doi.org/10.1016/S0960-9822(01)00325-6

Mikaelian, I., and A. Sergeant. 1992. A general and fast method to generate multiple site directed mutations. *Nucleic Acids Res.* 20:376. http://dx.doi.org/10.1093/nar/20.2.376

Murray, A.W. 1989. Cyclin synthesis and degradation and the embryonic cell cycle. *J. Cell Sci. Suppl.* 12:65–76. http://dx.doi.org/10.1242/jcs.1989.Supplement_12.7

Murray, A.W., M.J. Solomon, and M.W. Kirschner. 1989. The role of cyclin synthesis and degradation in the control of maturation promoting factor activity. *Nature.* 339:280–286. http://dx.doi.org/10.1038/339280a0

Musacchio, A. 2015. The molecular biology of spindle assembly checkpoint signaling dynamics. *Curr. Biol.* 25:R1002–R1018. (published erratum appears in *Curr. Biol.* 2015. 25:3017) http://dx.doi.org/10.1016/j.cub.2015.08.051

Ouellette, M.M., D.L. Aisner, I. Savre-Train, W.E. Wright, and J.W. Shay. 1999. Telomerase activity does not always imply telomere maintenance. *Biochem. Biophys. Res. Commun.* 254:795–803. http://dx.doi.org/10.1006/bbrc.1998.0114

Pagliuca, F.W., M.O. Collins, A. Lichawska, P. Zegerman, J.S. Choudhary, and J. Pines. 2011. Quantitative proteomics reveals the basis for the biochemical specificity of the cell-cycle machinery. *Mol. Cell.* 43:406–417. http://dx.doi.org/10.1016/j.molcel.2011.05.031

Petri, E.T., A. Errico, L. Escobedo, T. Hunt, and R. Basavappa. 2007. The crystal structure of human cyclin B. *Cell Cycle.* 6:1342–1349. http://dx.doi.org/10.4161/cc.6.11.4297

Pines, J. 2006. Mitosis: a matter of getting rid of the right protein at the right time. *Trends Cell Biol.* 16:55–63. http://dx.doi.org/10.1016/j.tcb.2005.11.006

Pines, J., and T. Hunter. 1991. Human cyclins A and B1 are differentially located in the cell and undergo cell cycle-dependent nuclear transport. *J. Cell Biol.* 115:1–17. http://dx.doi.org/10.1083/jcb.115.1.1

Reddy, S.K., M. Rape, W.A. Margansky, and M.W. Kirschner. 2007. Ubiquitination by the anaphase-promoting complex drives spindle checkpoint inactivation. *Nature.* 446:921–925. http://dx.doi.org/10.1038/nature05734

Robinson, J.T., H. Thorvaldsdóttir, W. Winckler, M. Guttman, E.S. Lander, G. Getz, and J.P. Mesirov. 2011. Integrative genomics viewer. *Nat. Biotechnol.* 29:24–26. http://dx.doi.org/10.1038/nbt.1754

Sackton, K.L., N. Dimova, X. Zeng, W. Tian, M. Zhang, T.B. Sackton, J. Meaders, K.L. Pfaff, F. Sigoillot, H. Yu, et al. 2014. Synergistic blockade of mitotic exit by two chemical inhibitors of the APC/C. *Nature.* 514:646–649. http://dx.doi.org/10.1038/nature13660

Salmela, A.L., and M.J. Kallio. 2013. Mitosis as an anti-cancer drug target. *Chromosoma.* 122:431–449. http://dx.doi.org/10.1007/s00412-013-0419-8

Schneider, C.A., W.S. Rasband, and K.W. Eliceiri. 2012. NIH Image to ImageJ: 25 years of image analysis. *Nat. Methods.* 9:671–675. http://dx.doi.org/10.1038/nmeth.2089

Shabbeer, S., D. Omer, D. Berneman, O. Weitzman, A. Alpaugh, A. Pietraszkiewicz, S. Metsuyanim, A. Shainskaya, M.Z. Papa, and R.I. Yarden. 2013. BRCA1 targets G2/M cell cycle proteins for ubiquitination and proteasomal degradation. *Oncogene.* 32:5005–5016. http://dx.doi.org/10.1038/onc.2012.522

Shaham, S. 2009. galign: a tool for rapid genome polymorphism discovery. *PLoS One.* 4:e7188. http://dx.doi.org/10.1371/journal.pone.0007188

Sonneville, R., and P. Gönczy. 2004. *Zyg-11* and *cul-2* regulate progression through meiosis II and polarity establishment in *C. elegans*. *Development.* 131:3527–3543. http://dx.doi.org/10.1242/dev.01244

Soucy, T.A., P.G. Smith, M.A. Milhollen, A.J. Berger, J.M. Gavin, S. Adhikari, J.E. Brownell, K.E. Burke, D.P. Cardin, S. Critchley, et al. 2009. An inhibitor of NEDD8-activating enzyme as a new approach to treat cancer. *Nature.* 458:732–736. http://dx.doi.org/10.1038/nature07884

Starostina, N.G., J.M. Lim, M. Schvarzstein, L. Wells, A.M. Spence, and E.T. Kipreos. 2007. A CUL-2 ubiquitin ligase containing three FEM proteins degrades TRA-1 to regulate *C. elegans* sex determination. *Dev. Cell.* 13:127–139. http://dx.doi.org/10.1016/j.devcel.2007.05.008

Stemmann, O., H. Zou, S.A. Gerber, S.P. Gygi, and M.W. Kirschner. 2001. Dual inhibition of sister chromatid separation at metaphase. *Cell.* 107:715–726. http://dx.doi.org/10.1016/S0092-8674(01)00603-1

Storchova, Z., and C. Kuffer. 2008. The consequences of tetraploidy and aneuploidy. *J. Cell Sci.* 121:3859–3866. http://dx.doi.org/10.1242/jcs.039537

Sulston, J., and J. Hodgkin. 1988. Methods. *In* The Nematode *Caenorhabditis elegans*. W.B. Wood, editor. Cold Spring Harbor Laboratory, Cold Spring Harbor, New York. 587–606.

Surana, U., A. Amon, C. Dowzer, J. McGrew, B. Byers, and K. Nasmyth. 1993. Destruction of the CDC28/CLB mitotic kinase is not required for the metaphase to anaphase transition in budding yeast. *EMBO J.* 12:1969–1978.

Timmons, L., D.L. Court, and A. Fire. 2001. Ingestion of bacterially expressed dsRNAs can produce specific and potent genetic interference in *Caenorhabditis elegans*. *Gene.* 263:103–112. http://dx.doi.org/10.1016/S0378-1119(00)00579-5

Uhlmann, F., F. Lottspeich, and K. Nasmyth. 1999. Sister-chromatid separation at anaphase onset is promoted by cleavage of the cohesin subunit Scc1. *Nature.* 400:37–42. http://dx.doi.org/10.1038/21831

van der Voet, M., M.A. Lorson, D.G. Srinivasan, K.L. Bennett, and S. van den Heuvel. 2009. *C. elegans* mitotic cyclins have distinct as well as overlapping functions in chromosome segregation. *Cell Cycle.* 8:4091–4102. http://dx.doi.org/10.4161/cc.8.24.10171

van Zon, W., J. Ogink, B. ter Riet, R.H. Medema, H. te Riele, and R.M. Wolthuis. 2010. The APC/C recruits cyclin B1-Cdk1-Cks in prometaphase before D box recognition to control mitotic exit. *J. Cell Biol.* 190:587–602. http://dx.doi.org/10.1083/jcb.200912084

Vassilev, L.T., C. Tovar, S. Chen, D. Knezevic, X. Zhao, H. Sun, D.C. Heimbrook, and L. Chen. 2006. Selective small-molecule inhibitor reveals critical mitotic functions of human CDK1. *Proc. Natl. Acad. Sci. USA.* 103:10660–10665. http://dx.doi.org/10.1073/pnas.0600447103

Vasudevan, S., N.G. Starostina, and E.T. Kipreos. 2007. The *Caenorhabditis elegans* cell-cycle regulator ZYG-11 defines a conserved family of CUL-2 complex components. *EMBO Rep.* 8:279–286. http://dx.doi.org/10.1038/sj.embor.7400895

Wang, R., Z. Kaul, C. Ambardekar, T.G. Yamamoto, K. Kavdia, K. Kodali, A.A. High, and R. Kitagawa. 2013. HECT-E3 ligase ETC-1 regulates securin and cyclin B1 cytoplasmic abundance to promote timely anaphase during meiosis in *C. elegans*. *Development.* 140:2149–2159. http://dx.doi.org/10.1242/dev.090688

Wieser, S., and J. Pines. 2015. The biochemistry of mitosis. *Cold Spring Harb. Perspect. Biol.* 7:a015776. http://dx.doi.org/10.1101/cshperspect.a015776

Zeng, X., F. Sigoillot, S. Gaur, S. Choi, K.L. Pfaff, D.C. Oh, N. Hathaway, N. Dimova, G.D. Cuny, and R.W. King. 2010. Pharmacologic inhibition of the anaphase-promoting complex induces a spindle checkpoint-dependent mitotic arrest in the absence of spindle damage. *Cancer Cell.* 18:382–395. http://dx.doi.org/10.1016/j.ccr.2010.08.010

Zou, H., T.J. McGarry, T. Bernal, and M.W. Kirschner. 1999. Identification of a vertebrate sister-chromatid separation inhibitor involved in transformation and tumorigenesis. *Science.* 285:418–422. http://dx.doi.org/10.1126/science.285.5426.418